

**Permafrost-wildfire interactions: Active layer thickness estimates for  
paired burned and unburned sites in northern high-latitudes**

Anna C. Talucci<sup>1</sup>, Michael M. Loranty<sup>2</sup>, Jean E. Holloway<sup>3</sup>, Brendan M. Rogers<sup>1</sup>, Heather D.  
Alexander<sup>4</sup>, Natalie Baillargeon<sup>1</sup>, Jennifer L. Baltzer<sup>5</sup>, Logan T. Berner<sup>6</sup>, Amy Breen<sup>7</sup>, Leya Brodt<sup>8</sup>,  
Brian Buma<sup>9, 10</sup>, Jacqueline Dean<sup>1</sup>, Clement J. F. Delcourt<sup>11</sup>, Lucas R. Diaz<sup>11</sup>, Catherine M. Dieleman<sup>12</sup>,  
Thomas A. Douglas<sup>13</sup>, Gerald V. Frost<sup>14</sup>, Benjamin V. Gaglioti<sup>15</sup>, Rebecca E. Hewitt<sup>16</sup>, Teresa  
Hollingsworth<sup>17,18</sup>, M. Torre Jorgenson<sup>19</sup>, Mark J. Lara<sup>20</sup>, Rachel A. Loehman<sup>21</sup>, Michelle C. Mack<sup>22</sup>,  
Kristen L. Manies<sup>23</sup>, Christina Minions<sup>1</sup>, Susan M. Natali<sup>1</sup>, Jonathan A. O'Donnell<sup>24</sup>, David Olefeldt<sup>25</sup>,  
Alison K. Paulson<sup>26</sup>, Adrian V. Rocha<sup>27</sup>, Lisa B. Saperstein<sup>28</sup>, Tatiana A. Shestakova<sup>29, 30, 1</sup>, Seeta  
Sistla<sup>31</sup>, Oleg Sizov<sup>32</sup>, Andrey Soromotin<sup>8</sup>, Merritt R. Turetsky<sup>33</sup>, Sander Veraverbeke<sup>11</sup>, Michelle A.  
Walvoord<sup>34</sup>

<sup>1</sup> Woodwell Climate Research Center, Falmouth, MA, 02540-1644, USA  
<sup>2</sup> Department of Geography, Colgate University, Hamilton, NY, 13346, USA  
<sup>3</sup> Department of Geography, Environment and Geomatics, University of Ottawa, Ottawa, K1N 6N5, Canada  
<sup>4</sup> College of Forestry, Wildlife, and Environment, Auburn University, Auburn, AL, 36949, USA  
<sup>5</sup> Biology Department, Wilfrid Laurier University, Waterloo, ON, N2L 3C5, Canada  
<sup>6</sup> School of Informatics, Computing, and Cyber Systems, Northern Arizona University, Flagstaff, AZ, 86011, USA  
<sup>7</sup> International Arctic Research Center, University of Alaska Fairbanks, Fairbanks, AK, 99775-7340, USA  
<sup>8</sup> Tyumen State University, Tyumen, 625003, Russia  
<sup>9</sup> Integrative Biology, University of Colorado (Denver), Boulder, CO, 80304, USA  
<sup>10</sup> Environmental Defense Fund, Boulder, CO 80302, USA  
<sup>11</sup> Faculty of Science, Vrije Universiteit Amsterdam, Amsterdam, 1081 HV, The Netherlands  
<sup>12</sup> School of Environmental Sciences, University of Guelph, Guelph, ON, N3H3Y8, Canada  
<sup>13</sup> U.S. Army Cold Regions Research and Engineering Laboratory, Fort Wainwright, AK, 99703, USA  
<sup>14</sup> Alaska Biological Research, Inc., Fairbanks, AK, 99708, USA  
<sup>15</sup> Water and Environmental Research Center, University of Alaska Fairbanks, Fairbanks, AK, 99775, USA  
<sup>16</sup> Department of Environmental Studies, Amherst College, Amherst, MA, 01002, USA  
<sup>17</sup> Pacific Northwest Research Station, USDA Forest Service, University of Alaska Fairbanks, Fairbanks, AK, 99708, USA  
<sup>18</sup> Aldo Leopold Wilderness Research Institute, Rocky Mountain Research Station, Missoula MT, 59801  
<sup>19</sup> Alaska Ecoscience, Fairbanks, AK, 99775, USA  
<sup>20</sup> Department(s) of Plant Biology and Geography, University of Illinois Urbana-Champaign, Urbana, IL, 61801, USA  
<sup>21</sup> U.S. Geological Survey, Alaska Science Center, Anchorage, AK, 99508, USA  
<sup>22</sup> Center for Ecosystem Science and Society and Department of Biological Sciences, Northern Arizona University, Flagstaff, AZ, 86001, USA  
<sup>23</sup> U.S. Geological Survey, Moffett Field, 94035, USA  
<sup>24</sup> Arctic Network, National Park Service, Anchorage, AK, 99501, USA  
<sup>25</sup> Department of Renewable Resources, University of Alberta, Edmonton, AB, T6G 2G7, Canada  
<sup>26</sup> Humboldt-Toiyabe National Forest, U.S. Forest Service, Sparks, NV, 89431, USA  
<sup>27</sup> Department of Biological Sciences, University of Notre Dame, Notre Dame, IN, 46556, USA  
<sup>28</sup> Alaska Regional Office, U.S. Fish and Wildlife Service, Anchorage, AK, 99503, USA  
<sup>29</sup> Department of Agricultural and Forest Sciences and Engineering, University of Lleida, Av. Alcalde Rovira Roure 191, Lleida, Catalonia 25198, Spain

44 <sup>30</sup> Joint Research Unit CTFC–AGROTECNIO–CERCA, Av. Alcalde Rovira Roure 191, Lleida, Catalonia 25198, Spain  
45 <sup>31</sup> Natural Resources Management & Environmental Sciences, Cal Poly, San Luis Obispo, CA, 93401, USA  
46 <sup>32</sup> Oil and Gas Research Institute RAS, Moscow, 119333, Russia  
47 <sup>33</sup> Renewable and Sustainable Energy Institute, Department of Ecology and Evolutionary Biology, University of Colorado  
48 Boulder, Boulder, CO, 80309-0552, USA  
49 <sup>34</sup> U.S. Geological Survey, Earth System Processes Division, Denver, CO, 80225, USA  
50

51 Correspondence to: Anna C. Talucci ([atalucci@woodwellclimate.org](mailto:atalucci@woodwellclimate.org))

52  
53  
54  
55 **Abstract.** As the northern high latitude permafrost zone experiences accelerated warming, permafrost has become vulnerable  
56 to widespread thaw. Simultaneously, wildfire activity across northern boreal forest and Arctic/subarctic tundra regions impact  
57 permafrost stability through the combustion of insulating organic matter, vegetation and post-fire changes in albedo. Efforts  
58 to synthesise the impacts of wildfire on permafrost are limited and are typically reliant on antecedent pre-fire conditions. To  
59 address this, we created the FireALT dataset by soliciting data contributions that included thaw depth measurements, site  
60 conditions, and fire event details with paired measurements at environmentally comparable burned and unburned sites. The  
61 solicitation resulted in 52,466 thaw depth measurements from 18 contributors across North America and Russia. Because thaw  
62 depths were taken at various times throughout the thawing season, we also estimated end of season active layer thickness  
63 (ALT) for each measurement using a modified version of the Stefan equation. Here, we describe our methods for collecting  
64 and quality checking the data, estimating ALT, the data structure, strengths and limitations, and future research opportunities.  
65 The final dataset includes 48,669 ALT estimates with 32 attributes across 9,446 plots and 157 burned/unburned pairs that  
66 span Canada, Russia, and the United States. The data span fire events from 1900 to 2022 with measurements collected from  
67 2001 to 2023. Time since fire ranges from zero to 114 years. The FireALT dataset addresses a key challenge: the ability to  
68 assess impacts of wildfire on ALT when measurements are taken at various times throughout the thaw season depending on  
69 the time of field campaigns (typically June through August) by estimating ALT at the end of season maximum. This dataset  
70 can be used to address understudied research areas particularly algorithm development, calibration, and validation for evolving  
71 process-based models as well as extrapolating across space and time, which could elucidate permafrost-wildfire interactions  
72 under accelerated warming across the high northern latitude permafrost zone. The FireALT dataset is available through the  
73 Arctic Data Center.  
74

77 **1 Introduction**

78 Permafrost, defined as ground that remains at or below 0°C for two or more consecutive years, has become vulnerable to  
79 widespread thaw in response to rapid climate warming at high latitudes. Permafrost temperatures have increased over the last  
80 30 years (Romanovsky et al., 2010, Smith et al., 2022, Calvin et al., 2023) resulting in the thickening of the active layer, which  
81 is the uppermost, seasonally thawed layer (Harris and Permafrost Subcommittee, Associate Committee on Geotechnical  
82 Research, National Research Council of Canada, 1988, Bonnaventure and Lamoureux 2013). Widespread permafrost thaw and

Deleted: 47,952

Deleted: (27,747 burned, 20,205 unburned)

Deleted: 9,432

Deleted: 388 sites

Deleted:

Deleted: with 32 attributes

Deleted: . There are

Deleted: 157

Deleted: 193 unique paired burned/unburned

Deleted: pairs

Deleted: sites spread across 12 ecozones

Formatted: Font: Not Bold

Formatted: Font: Not Bold

Formatted: Font: Not Bold

94 increases in active layer thickness are expected under future climate conditions (Smith and Burgess 2004, Zhang et al., 2008,  
95 Derksen et al., 2019, Peng et al., 2023), and these processes are expected to release large amounts of soil carbon to the  
96 atmosphere as greenhouse gas emissions (Schaefer et al., 2014, Gasser et al., 2018, Knoblauch et al., 2018, Yokohata et al.,  
97 2020, Natali et al., 2021, Schuur et al., 2022, See et al., 2024). Changes to permafrost, particularly near-surface permafrost  
98 and the active layer, have important implications for ecology, forestry, hydrology, biogeochemistry, climate feedbacks,  
99 engineering, traditional livelihoods, and community safety (Anisimov and Reneva 2006, O'Donnell et al., 2011b, Rocha and  
100 Shaver 2011, Bret-Harte et al., 2013, Hugelius et al., 2014, Jones et al., 2015, Li et al., 2019, Turetsky et al., 2020, Gibson et  
101 al., 2021, Huang et al., 2024).

102

103 Climate change is also intensifying high-latitude wildfire regimes (Kasischke et al., 2010, de Groot et al., 2013, Zhang et al.,  
104 2015, Wotton et al., 2017, Hanes et al., 2019, McCarty et al., 2021, Descals et al., 2022, Phillips et al., 2022, Scholten et al.,  
105 2022, Zheng et al., 2023, Byrne et al., 2024). Wildfire activity shows interannual variability that is predominantly controlled  
106 by subseasonal drying and climate, where prolonged warm and dry conditions in conjunction with fuel accumulation may alter  
107 fire regimes and the seasonality of fire (York et al., 2020). The interaction between wildfire and permafrost results in both  
108 immediate and long-term effects on the surface energy balance and ground thermal regimes, as well as hydrologic cycling and  
109 soil and aquatic biogeochemistry (O'Donnell et al., 2011b, Rocha and Shaver 2011, Bret-Harte et al., 2013, Jones et al., 2015,  
110 Li et al., 2019, Hollingsworth et al., 2020, Holloway et al., 2020). These interactions also result in second-order greenhouse  
111 gas emissions (O'Donnell et al., 2011c, Jiang et al., 2015, Smith et al., 2015, Jones et al., 2015, Gibson et al., 2018, Li et al.,  
112 2019) by making stored soil carbon available for mineralization (O'Donnell et al., 2011c, Rocha and Shaver 2011, Bret-Harte  
113 et al., 2013, Hugelius et al., 2014, Jones et al., 2015, Li et al. 2019). Biomass combustion during fires removes the insulating  
114 surface vegetation (i.e., moss, lichen, low growing shrubs) and soil organic matter, typically reduces evapotranspiration (Rouse  
115 1976, Amiro 2001, Chambers and Chapin 2002, Chambers et al., 2005, Amiro et al., 2006, [Chebykina et al., 2022](#), [Fedorov,](#)  
116 [2022](#)), and reduces short-term albedo [during thaw season](#), resulting in increases in the ground heat flux and the expansion of  
117 the active layer ([Moskalenko 1999](#), Rocha et al., 2012, Jafarov et al., 2013, Nosssov et al., 2013, Jiang et al., 2015, Douglas et  
118 al., 2016, Fisher et al., 2016, Gibson et al., 2018). Similarly, tree canopy removal reduces shading in the summer and results  
119 in more snow on the ground in the winter, both leading to higher surface soil temperatures and expansion of the active layer  
120 into near-surface permafrost, [which has been shown across North America](#) (Rocha et al., 2012, Jafarov et al., 2013, Jiang et  
121 al., 2015, Zhang et al., 2015, Douglas et al., 2016, Fisher et al., 2016, Gibson et al., 2018) [and Eurasia](#) ([Moskalenko 1999](#),  
122 [Lytkina, 2008](#), [Kirdyanov et al., 2020](#), [Heim et al., 2021](#), [Fedorov, 2022](#), [Petrov et al., 2022](#)). In contrast, across [North](#)  
123 [American](#) Arctic tundra, shrub removal from wildfire results in thinner snow due to increased wind exposure, which causes a  
124 reduction of the active layer (Wang et al., 2012, Jones et al., 2024), [while Russian scientists note an expansion of the seasonal](#)  
125 [active layer that is dependent on vegetation communities](#) ([Moskalenko 1999](#), [Lytkina, 2008](#)).

126

Deleted: (i.e., the surface reflectance)

Deleted:

Deleted: .

130 Post-fire changes in the energy balance and subsequent increases in the active layer thickness have historically recovered to  
131 pre-fire conditions as vegetation succession occurred (Rouse 1976, Amiro 2001, Liu et al., 2005, Amiro et al., 2006), with a  
132 maximum active layer thickness often observed 5-10 years post-fire (Rocha et al., 2012, Holloway et al., 2020) but may extend  
133 up to 30 or more years post-fire (Gibson et al., 2018, Kirdyanov et al., 2020, Heim et al., 2021). However, this pattern of  
134 recovery may be changing alongside climate warming and shifting fire regimes (Brown et al., 2015), and may be further  
135 impacted by secondary disturbances (Hayes and Buma, 2021). For example, as wildfire burns across permafrost peatlands, not  
136 only is there a thicker and warmer active layer but an expansion of year-round unfrozen ground (i.e., taliks) and thermokarst  
137 bogs (Gibson et al., 2018). These changes in active layer thickness and hydrologic dynamics can constrain regeneration by  
138 prolonging vegetation recovery and inducing shifts in vegetation composition and structure (Baltzer et al., 2014, Dearborn et  
139 al., 2021). Further, near-surface permafrost degradation can lead to ground subsidence, which alters surface hydrology, often  
140 leading to water inundation and further degradation (Brown et al., 2015). Where wildfires burn across permafrost landforms  
141 (e.g., thermokarst, ice rich areas), deep and irreversible thawing could permanently alter the landscape (Burn and Lewkowicz  
142 1990, Lewkowicz 2007, Sannel and Kuhry 2011, Liljedahl et al., 2016, Rudy et al., 2017, Borge et al., 2017, Mamet et al.,  
143 2017, Fraser et al., 2018), releasing long stored soil carbon into the atmosphere (Schuur et al., 2015). Currently, emissions  
144 from fire-induced permafrost thaw are underestimated by the scientific community and climate models (Natali et al., 2021,  
145 Treharne et al., 2022, Schädel et al., 2024), an issue that is exacerbated by modelling challenges and uncertainties associated  
146 with permafrost carbon stocks (Hugelius et al., 2014, Turetsky et al., 2020). The change in active layer thickness over time is  
147 a critical diagnostic indicator of permafrost conditions (Brown et al., 2000, Shiklomanov et al., 2010) and a vital component  
148 of modelling carbon emissions from fire and non-fire related permafrost thaw.

150 To provide critical data that can be used for understanding and modelling impacts of wildfire on permafrost, we compiled a  
151 dataset of thaw depth measurements from paired burned and unburned sites across the northern high-latitude permafrost zone.  
152 This dataset is the first of its kind to focus on paired burned and unburned sites providing a circumpolar/boreal perspective.  
153 Climate and ecosystem conditions including drainage, vegetation, and soil characteristics control near-surface permafrost  
154 characteristics, and thus in order to detect an influence of wildfire it is necessary to have measurements either pre- and post-  
155 fire, or unburned control and burned nearby sites with otherwise similar ecosystem properties. Measuring ALT for paired  
156 unburned control and nearby burn sites is more realistic due to the stochasticity of wildfire. Further, unburned control sites  
157 provide a benchmark for understanding the impact of wildfire in these dynamic systems. Thaw depth increases over the course  
158 of the thawing season until it reaches its maximum depth, i.e., active layer thickness (ALT). This means that early to mid-  
159 season measurements do not capture the full depth of the thawed active layer. As such, the variability in thawing season and  
160 measurement timing makes it difficult to compare across space and time. Therefore, we standardised thaw depths taken at  
161 different times throughout the thawing season, which resulted in an estimated dataset of ALT. Further, capturing the maximum  
162 ALT aids in establishing the full scope of permafrost change because it is a critical indicator of thaw dynamics. Depending on  
163 the location ALT could occur anywhere from August through November. The overarching goal is to generate a synthesised  
164 data set of ALT for burned/unburned pairs. To achieve this, we had four main objectives for the paper: 1) describe how the  
165 data was collected and synthesised for thaw depth measurements of burned sites with paired unburned sites, 2) describe how  
166 we standardised thaw depth measurements to end-of-season ALT with estimates of uncertainty, 3) provide details on how to  
167 aggregate data to plot, site, and paired burned/unburned means, and provide a summary of the data set, and 4) discuss the  
168 strengths and limitations of the dataset, along with its potential uses.

**Deleted:** site-level data

**Deleted:** a general overview of this aggregated data

**Deleted:** This paper provides a description of the data solicitation and compilation, the process for standardising the measurements, and general descriptive statistics on the dataset. Finally, we describe the strengths and limitations of the dataset, future research directions, and protocols for accessing and using this dataset.

**Deleted:** ¶

177 2 Data and Methods

178 2.1 Data Solicitation and Quality Screening

179 To assemble a dataset capable of widely characterising the influence of wildfire on permafrost, we solicited field measurements  
180 of thaw depth from paired burned and unburned sites from researchers working in boreal forest and tundra ecosystems. Thaw  
181 depth refers to depth or thickness of the unfrozen surface soil layer anytime during the thawing season. [The data sets that](#)  
182 [contribute to this synthesis were](#) obtained by measuring depth to refusal using a graduated steel probe [\(Brown et al., 2000\)](#). [A](#)  
183 [steel probe is a typical means of measurements, however, there is potential for error introduced by issues such as identifying](#)  
184 [the freeze-thaw boundary, soil variability, subsidence, user bias](#) [\(Brown et al., 2000, Bonnaventure and Lamoureux, 2013,](#)  
185 [Strand et al., 2021, Scheer et al., 2023\)](#). A critical component of the data required an ecologically appropriate unburned site(s)  
186 within close proximity that shared similar dominant vegetation, drainage, and climatic conditions to be paired with one or  
187 more burned sites, meaning the burned site would have had similar pre-fire conditions to the unburned site. We began by  
188 soliciting data from members of the Permafrost Carbon Network and their collaborators and then used literature review to  
189 identify additional contributors. Data contributors were required to submit metadata (Table S1) and data via a Google form  
190 with required attributes that included their last name, country where data were collected, latitude, longitude, biome, vegetation  
191 cover class, site identifier, plot identifier, year data were collected, month data were collected, day data was collected, fire  
192 identifier, fire year, whether the site was burned or unburned, organic layer depth, thaw depth, whether the probe hit rocks,  
193 whether the depth was greater than the probe, contributors assigned a designation of ‘thaw’ or ‘active’ to indicate early-mid or  
194 late season measurements respectively, slope, topographic position, pairing, and whether surface water was present. The  
195 solicitation resulted in the contribution of 18 datasets with 52,466 thaw depth measurements covering portions of the northern  
196 high-latitude permafrost zones in Canada, Russia, and the United States (Table 1, Fig. 1).

198 Table 1. Brief description of the data contributions. Table includes the last name of the contributor, geographic location of the data,  
199 fire years that were sampled and relevant citations associated with the data.

Contributor	Country	Location description	Biome	Ecozone	Fire years	Citations
Baillargeon	United States	Yukon Kuskokwim Delta, AK, USA	Tundra	Beringia lowland tundra	1972, 2015	Baillargeon et al., 2022
Breen	United States	Kougarok Fire Complex on the Seward Peninsula, AK, USA	Tundra	Beringia upland tundra	1971, 1982, 2002, 2011	Hollingsworth et al., 2020, 2021
Buma	United States	Central Alaska black spruce forest	Boreal	Interior Alaska-Yukon lowland taiga	2005	B. Buma, University of Colorado (Denver), unpublished data, 2005
Delcourt	Russia	Northeast Siberia, Russia	Boreal	East Siberian taiga	2018	Delcourt et al., 2024

Deleted: , and is typically

Commented [MOU1]: Updated from original manuscript

Deleted: Tundra f

Deleted: c

Diaz	United States	Alaska, USA	Boreal; Tundra	Interior Alaska-Yukon lowland taiga; Beringia lowland tundra	2022	L.R. Diaz, Vrije Universiteit Amsterdam, unpublished data, 2022
Baltzer, Dieleman, Turetsky	Canada	Northwest Territories, Canada	Boreal	Muskwa-Slave Lake taiga; Northern Canadian Shield taiga; Northwest Territories taiga	1940, 1960, 1969, 1971, 1972, 1973, 1980, 1981, 2011, 2013, 2014	Dieleman et al., 2022
Douglas, Jorgenson	United States	Interior Boreal near Fairbanks, AK, USA	Boreal	Interior Alaska-Yukon lowland taiga	2005-2020	Douglas et al., 2020
Frost	United States	central Yukon-Kuskokwim Delta, western Alaska	Tundra	Beringia lowland tundra	1971, 1972, 1985, 2006, 2007, 2015	Frost et al., 2020
Gaglioti	United States	The Noatak watershed, which drains the southwestern flank of the Brooks Range in northwestern Alaska	Tundra	Arctic foothills tundra	1972, 1984	Gaglioti et al., 2021
Holloway	Canada	Taiga Plains and Taiga Shield ecozones near Yellowknife, Canada	Boreal	Muskwa-Slave Lake taiga; Northern Canadian Shield taiga; Northwest Territories taiga	2014, 2015	Holloway et al., 2024
Loranty	Russia	Northeastern Siberia Larch forests	Tundra	Chukchi Peninsula tundra	1972	Loranty, et al., 2014
Manics	United States	Interior Alaska, black spruce forests	Boreal	Interior Alaska-Yukon lowland taiga	1999	Harden et al., 2006
Natali	United States	Bonanza Creek, Alaska USA; Anaktuvuk River fire, AK USA; Yukon Kuskokwim Delta, AK	Boreal; Tundra	Interior Alaska-Yukon lowland taiga; Interior Yukon-Alaska alpine tundra; Arctic foothills tundra; Beringia lowland tundra	1983, 2003, 2004, 2007, 2015	Natali et al., 2016, 2018, Natali 2018
O'Donnell	United States	Interior Boreal, AK, USA	Boreal; Tundra	Interior Alaska-Yukon lowland taiga; Interior Yukon-Alaska alpine tundra	1966, 1967, 1990, 2003, 2004	O'Donnell et al., 2009, 2011a, 2011b, 2013
Olefeldt	Canada	Western Boreal Canada	Boreal	Muskwa-Slave Lake taiga; Northwest Territories taiga	1964, 1967, 1975, 1982, 1984, 1995, 2000, 2006, 2007, 2008, 2012, 2013, 2014, 2019	Gibson et al., 2018
Paulson, Alexander	Russia	Northeastern Siberia near Cherskiy, Russia, and Yakutsk, Russia	Boreal	East Siberian taiga; Northeast Siberian taiga	1983, 1984, 1990, 2001, 2002, 2003, 2010, 2015	Alexander et al., 2020
Rocha	United States	North Slope of Alaska	Tundra	Arctic foothills tundra	1977, 1993, 2001, 2007	Rocha and Shaver, 2011

Sizov	Russia	Northwestern Russia, Nadym region of the Yamal-Nenets Autonomous Okrug	Tundra	Yamal-Gydan tundra	2016	Sizov et al., 2020
-------	--------	---------------------------------------------------------------------------------	--------	--------------------	------	--------------------



205 **Figure 1. Map of the northern high latitude permafrost zone showing the percent of thaw depth measurements by ecozones (circle**  
206 **colour, Dinerstein et al., 2017) with the extent of continuous, discontinuous, and sporadic permafrost shown in shades of blue (Brown**  
207 **et al., 1998). Points are sized and labelled with the percent of measurements within each ecozone. The Arctic circle is shown with the**  
208 **thick dashed black line.**

209  
210 We screened the data for issues with units, sign convention, coordinates, and data type (e.g., factor, integer). Where we required  
211 categorical variables, we ensured these were spelled in a consistent manner and that the correct unique number of variables  
212 were returned. We mapped the data to check inaccurate site coordinates and checked discrepancies, such as missing negative  
213 signs from longitude, with contributors. We used histograms of measurement depths to identify any outliers in the data, several  
214 of which were removed after confirming with the contributors that they were the result of typographic errors. Data contributors  
215 were asked to note if any measurements hit rock, and, when noted, these observations were excluded from the final dataset.

216

## 217 **2.2 Estimating Active Layer Thickness**

218 Over the course of the growing season, the depth of the thawing front increases as the active layer expands to its maximum.  
219 Therefore, measurements taken throughout the thaw season are not directly comparable with one another. Therefore, we  
220 standardised thaw depths taken at different times throughout the thawing season, which resulted in an estimated dataset of  
221 ALT. To do so, we estimated ALT using a modified version of the Stefan equation, used by Holloway and Lewkowicz (2020)  
222 and described by Riseborough et al. (2018) and Bonnaventure and Lamoureux (2013). Estimating ALT (Fig. 2) allows thaw  
223 depth measurements collected during different times in the growing season to be comparable and used to understand the full  
224 effects of wildfire on the active layer across paired sites in a given measurement year and for some of the sites across multiple  
225 years.



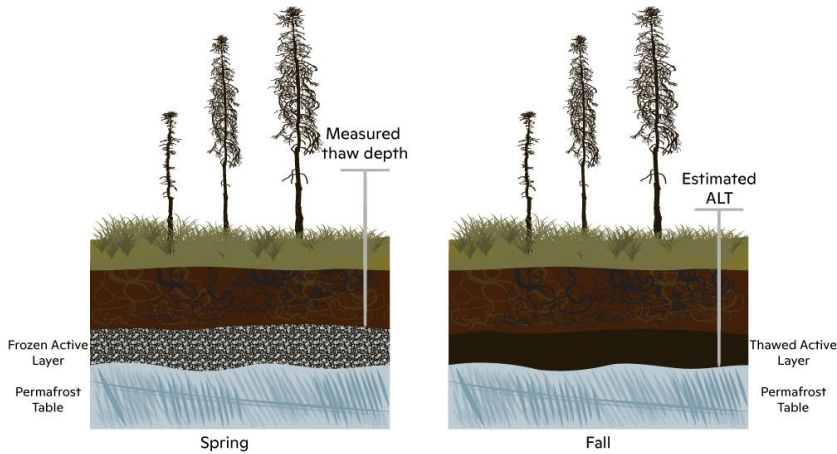


**Figure 2. Diagram of early season thaw depth measurement versus late season active layer thickness. The active layer expands during the thawing season reaching its maximum thickness between August and November depending on the location.**

ALT was estimated based on air thawing degree days (TDD; i.e., days above zero degrees Celsius during the thawing season). Others have shown a correlation between TDD and ALT (e.g., Strand et al., 2021). Daily mean air temperatures were extracted from ERA5-Land daily aggregates (Muñoz Sabater 2019) accessed through Google Earth Engine (Gorelick et al., 2017). Instrumental air temperature data are sparse across the northern high-latitude regions. We selected the ERA5-Land (Muñoz Sabater, 2019) dataset since it is available for the full region and time series, accessible through Google Earth Engine, and has been evaluated against meteorological station data (Rantanen et al., 2023, Clelland et al. 2024). Across the circum-Arctic and Asian boreal ERA5-Land validation studies indicate a warming bias in winter months of a half a degree Celsius (Rantanen et al., 2023, Clelland et al. 2024), whereas validation studies in summer indicate a slight cooling trend of ~0.2 degrees Celsius (Rantanen et al., 2023). Due to the scarcity of meteorological stations across the Northwestern Territories, we provide additional validation for air temperature data from ERA5-Land using shielded air temperatures at a height of 1.5 m that were measured at six sites using Onset Corporation (USA) Hobo Pro U23-003 loggers (accuracy  $\pm 0.21^{\circ}\text{C}$ ; precision  $\pm 0.02^{\circ}\text{C}$ ). All air temperature data were aggregated from 2-hour samples to daily averages and sites included thaw depth measurements (Holloway 2020). We calculate Pearson's correlation coefficient ( $R$ ), bias (defined as the summation of modelled minus measured divided by the number of data points), and the root mean square error (RMSE). The correlation is ~0.99, with a warming bias of 0.54 degrees Celsius, and a RMSE of 2.23 degrees Celsius (Fig. S2).

First, we defined the end of the thaw season for each measurement location and year based on when the five-day mean daily air temperature shifted from above- to below-freezing. We then subtracted 14 days from the end-of-season date to account for

the lag between surface freezing and the refreezing of the bottom of the active layer. Typically, the active layer begins to freeze upward while the air temperature is still above zero, requiring approximately 7-14 days until the surface freezes (Osterkamp and Burn 2002). Following the Stefan equation (Freitag and McFadden, 1997), we calculate (A) as the square root of the sum of daily mean air temperature TDD prior to the day of year of the field measurement (i.e., thaw depth), as in Eq. (1):

$$A = \sqrt{\sum_{TDD \text{ thaw depth}=1}^n TDD \text{ Thaw depth}}, \quad (1)$$

We calculate (B) as the square root of the sum of daily mean air temperature TDD (i.e., days above zero degrees Celsius) prior to the end of thaw season day of year (i.e., ALT) Eq. (2):

$$B = \sqrt{\sum_{TDD \text{ ALT}=1}^n TDD \text{ ALT}}, \quad (2)$$

Finally, we multiplied the field measured depth by the ratio of the first two equations to calculate the estimated ALT Eq. (3):

$$\text{estimated ALT} = \text{field measured depth} \times (B \div A), \quad (3)$$

An example of the calculation for two sites is provided in Table 3 and shown in Fig. 3.

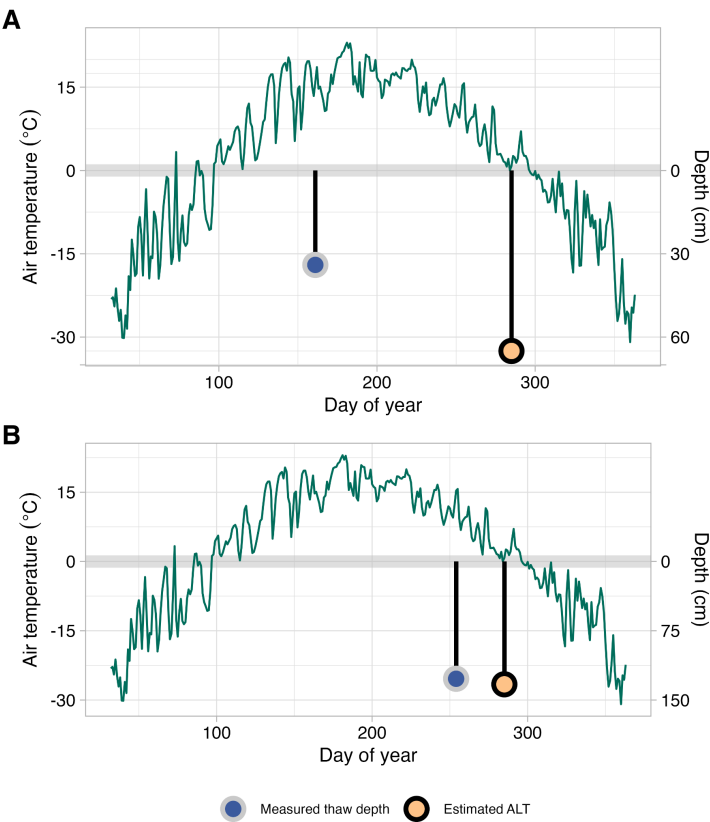


Figure 3. An example of estimating active layer thickness from two *in situ* thaw depth measurements using seasonal air temperature. Air temperature through the thawing season (green line) for two separate sites, one with an early-season thaw depth measurement (A) and a second with an end-of-season thaw depth measurement (B). For each site, we show the measured thaw depth (blue point) and estimated ALT depth (orange point) for the day of year either measured or estimated. The right y-axis shows thaw depth (cm), the left y-axis shows air temperature and the x-axis shows the day of the year.

Table 3. An example of estimating ALT using Equations 1-3 from two *in situ* thaw depth measurements at two sites (A and B) using the same data as in Fig. 3.

	Site	A	B
Data contribution	Timing of measurement	Early season	End of Season

273  
274  
275  
276  
277  
278  
  
279  
280  
281  
282  
283  
284  
285  
286  
287  
288  
289  
  
290  
291  
292  
293  
294  
295  
296  
297

	Year	2015	2015
	Month	6	9
	Day	10	11
	Day of year	161	254
	Measurement depth (cm)	34	127
Calculated from ERA5 data extracted based on location	Day of year first of five consecutive days at zero	299	299
	Day of year to estimate ALT	285	285
	Eq.1	25.25	45.95
	Eq.2	48.03	48.03
Estimated ALT	Eq.3 (cm)	65	133

Estimates were excluded for observations that hit rock, were greater than the depth of the measurement probe, or were missing the day of month (Table S2). We were unable to convert every early season thaw depth to ALT if the date of measurement was not preceded by at least one day above zero degrees Celsius, in which case these measurements were removed from the estimated dataset. Ultimately, 48,669 of the original 52,466 measurements were included in the estimated dataset.

Deleted: 47,952

2.3 Quantify uncertainty of estimated ALT

We quantify uncertainty in our estimates of ALT by calculating Pearson’s correlation coefficient (*R*), bias (defined as the summation of modelled minus measured divided by the number of data points), and the Root Mean Square Error (RMSE). The bias indicates whether estimated ALT is over or underestimated, while the RMSE provides an average error regardless of sign. We used two data sets for this analysis from contributors that had repeat measurements from within a season for early/mid-season and late season at the same locations. These data sets differed as one was a subset of their data contributed to the data synthesis for the boreal near Yellowknife, Canada (N = 626; Holloway et al. 2024), whereas the other was used solely for quantifying uncertainty for tundra on the Seward Peninsula, AK (N = 37; Breen, unpublished). The tundra data was missing key meta data which precluded it from the synthesis. We used the early/mid-season measurements to estimate thaw depths for the date of the late season measurement (as opposed to the end of the thaw season defined using ERA5-Land) following the methodology described in Section 2.2, to quantify the uncertainty in the estimation process.

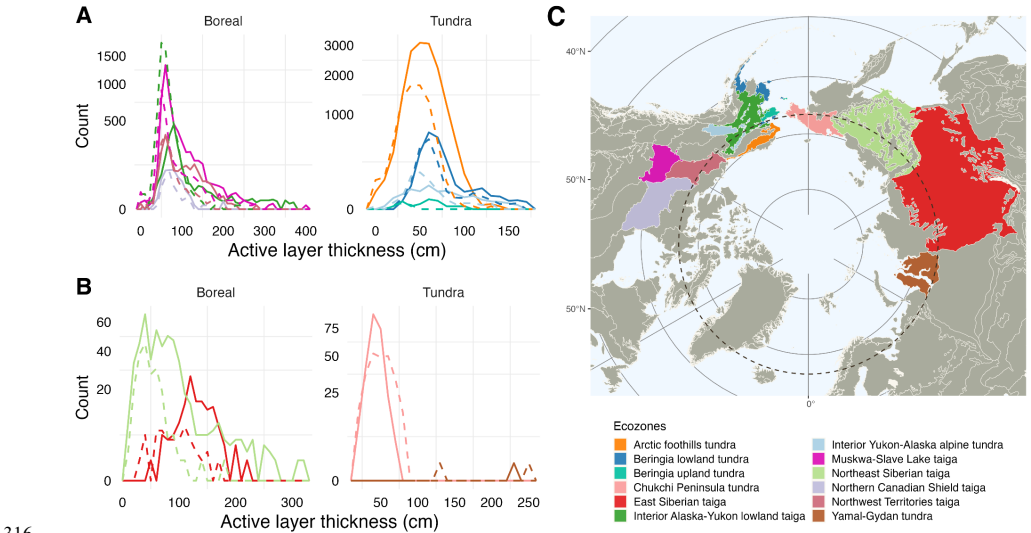
- Deleted: We used a separate
- Deleted: subset of
- Deleted: data
- Deleted: from two contributors that had repeat measurements from within a season for early/mid-season and late season at the same locations ...
- Deleted: set (n=626) that had repeat thaw depth measurements at the same location taken throughout the thaw season
- Deleted: data from the boreal near Yellowknife, Canada
- Deleted: (Holloway et al., 2024)
- Deleted: and data from the tundra on the Seward Peninsula, AK
- Deleted: .
- Deleted:

2.4 Spatial attributes

We added spatial attributes to the data through spatial joins. We generated a point shapefile using the latitude and longitude coordinates with the coordinate reference system (CRS) 4326 (i.e., WGS 84). We performed a spatial join to add ecozone data (Dinerstein et al., 2017), retaining the ecozone and biome names. We then performed a second spatial join with permafrost data (Brown et al., 1998), retaining permafrost extent (e.g., continuous, discontinuous, sporadic). We show the distribution of estimated ALT measurements by ecozone (Fig. 4). The spatial coverage, and hence inherent resolution, of these polygon products is much larger than the data points or any site-level aggregation. Due to the coarser resolution, data contributors designation of biome outweighed what was assigned through the spatial join. The small percentage of plots where the biome

was misassigned were visually inspected and found to be adjacent to the boundary with the matching biome and were manually reassigned (see code).

314  
315



316

Figure 4. Frequency distribution graphs showing estimated active layer thickness (cm) by ecozones split by North America (A) and Eurasia (B), solid line for burned distribution and dashed line for unburned distribution. Map of ecozones for location reference (C; Dinerstein et al., 2017). The y-axis is the count of measurements and the x-axis is the depth in centimetres. Both x- and y-axis vary by panel and y-axes are adjusted to show low counts.

## 2.5 Data structure and columns

The resulting dataset includes 32 attributes including attributes from the initial contribution, plus the attributes from the spatial joins and the derived ALT estimates all described in Table 4. The dataset is shared in comma separated values (csv) format with 48,669 rows and 32 columns. For missing values, we used 'NA' and '-9999', for character and numeric fields, respectively.

326

Table 4. Description of data attributes and data format. All attributes are included with the raw data. Attributes included with the plot level data are denoted with a \* and data from paired burned/unburned are denoted with a †.

328

Attribute	Format	Description
-----------	--------	-------------

Deleted: 47,952

plotId*	character	A unique identifier assigned by the data contributor to identify the field plot.
siteId*	character	Site name assigned by the data contributor specific to the fieldwork.
lastNm*†	character	Last name(s) of the person(s) contributing the data provided by the data contributor.
submitNm*†	character	Last name of the data contributor that submitted the form (single name only).
biome*†	character	Boreal (B) or tundra (T) assigned by the data contributor.
distur*†	character	Categorical variable to identify location as burned or unburned provided by the data contributor.
cntryId*†	character	Dropdown list of two-digit code: Russia (RU), USA (US), Canada (CA), Finland (FI), Norway (NO), Sweden (SE), Iceland (IS), Greenland (GL) assigned by the data contributor.
fireYr*†	integer	Four-digit year of when the fire event occurred provided by the data contributor.
fireId*†	character	Unique fire identifier assigned by the data contributor.
gtProbe*	character	Permafrost thaw depth exceeds (i.e., greater than [gt]) the length of probe yes (y) or no (n) provided by the data contributor.
hitRock*	character	Probe hit rock yes (y) or no (n) provided by the data contributor.
lat*	float	Latitude in decimal degrees in WGS 84 provided by the data contributor.
lon*	float	Longitude in decimal degrees in WGS 84 provided by the data contributor.
year*†	integer	Four-digit year the data were collected provided by the data contributor.
month	integer	Two-digit month (values 01-12 accepted) the data were collected provided by the data contributor.
day	integer	Day of month data were collected values( 1-31) provided by the data contributor.
orgDpth*	integer	Organic layer thickness measured from the ground/moss surface to the organic-mineral interface, as a site mean in cm, provided by the data contributor.
srfH2O*	character	A categorical variable describing if plot locations experience seasonal inundation (i.e., standing surface water during the early season but dry by late season). Seasonal inundation (Y: yes) or not (N: no) or unknown (U). Provided by the data contributor.
msrType	character	A categorical variable of thaw (T) or active (A). Active refers to active layer thickness (i.e., maximum seasonal thaw at the end of growing season), and thaw refers to thaw depth (i.e., less than seasonal maximum taken earlier than the end of thawing season). Provided by the data contributor.
msrDoy	integer	Day of year (DOY) for the day of measurement converted from YYYY-MM-DD.
msrDepth	float	The field measurement of the thaw depth or ALT in cm. Provided by the data contributor.
topoPos*	character	Categorical variable describing the topographic position of plot locations as upland (U), midslope (M), lowland (L). Provided by the data contributor.
slope*	integer	Numeric value indicating slope angle provided by the data contributor.
vegCvr*	character	Evergreen needle-leaf (EN); broadleaf deciduous (BD); deciduous needle-leaf (DN); mixed needle-leaf majority MNM; mixed (M); mixed broadleaf majority (MBM); barrens (B), graminoid tussock dominated (GT), graminoid non-tussock dominated (GNT), prostrate shrub dominated (P), erect-shrub dominated (S), and wetlands (W). Provided by the data contributor.
resBiome*	character	Biome assigned by spatial join with the Resolve data product ( <a href="#">vector data</a> ) 'BIOME_NAME' (Dinerstein et al., 2017).
resName*	character	Ecozone name assigned by spatial join with the Resolve data product ( <a href="#">vector data</a> ) 'ECO_NAME' (Dinerstein et al., 2017).
permaExtent*†	character	Permafrost extent ( <a href="#">vector data</a> ) assigned by spatial join with permafrost ground-ice map 'EXTENT' as C=continuous, D=discontinuous, S=sporadic (Brown et al., 1998).
estDoy*	integer	The day of year used to estimate ALT based on when the five-day mean daily air temperature shifted from above- to below-freezing.
estDepth*†	float	The estimated ALT in cm; calculated using air temperature from ERA5-Land and field measured thaw depth.
paired*†	character	Identifying code to pair unburned measurements to burned measurements provided by the data contributor.

tsf*	integer	Time since fire calculated by subtracting year from fireYr.
tsfClass*	character	Binned time since fire (tsf) classes in years as "unburned", "0-3", "4-10", "11-20", "21-40", ">40"
n*	integer	number of measurements used to calculate plot-level or pair burned/unburned means

2.6 Aggregating plot level data and pair burned to unburned data

While the main objective of the data synthesis is to provide paired burned/unburned ALT estimates, we also want to provide details on aggregating to the site/plot level. We aggregated plot and paired level data in R with ‘tidyverse’ (Wickham et al., 2019). Plot level data was aggregated using the ‘group\_by’ function aggregate using the following variables: data contributor (‘submitNm’), burned or unburned (‘distur’), site level identifier (‘siteId’), plot level identifier (‘plotId’), fire year (‘fireYr’), and year of measurement (‘year’), which captures both the spatial and temporal component of the data. We then calculated the mean ALT for each plot that includes 28 attributes, (see Table 4 for descriptions). Paired burned and unburned sites are a unique and defining characteristic of this dataset. Data contributors were required to provide details on how their burned measurements paired with unburned measurements. Characteristics of unburned plots were required to be representative of biogeoclimatic conditions prefire and within close proximity to their paired burned plot(s). The dataset includes a code to link burned with unburned sites (‘paired’). To aggregate at the paired level, we grouped by data contributor (‘submitNm’), burned or unburned (‘distur’), pairing code (‘paired’), year of the fire event (‘fireYr’), and can be further grouped by time since fire (‘tsf’). The paired burned/unburned data includes 13 attributes (Table 4).

3 Data summary

3.1 General Characteristics of the data

In total, the final dataset includes 48,669 observations from the original 52,466 observations across 9,446 plots and 388 sites. Thaw depth measurements are predominantly from North America, with 35,272 (19,739 burned, 15,533 unburned) in Alaska and 11,844 (7,553 burned, 4,291 unburned) in Canada, and 1,553 (998 burned, 555 unburned) in Russia. These *in situ* measurements were collected within the continuous, discontinuous, and sporadic permafrost zones (Fig. 1). Data were contributed with both burned and unburned paired sites with fire years ranging from 1900 to 2022 across 112 fire events. There are 193 unique paired burned/unburned measures based on pair id (76), fire year (37 unique years), fire events (63 unique events), and time since fire spread across 12 ecozones. There are 21,589 estimated observations across the boreal forests/taiga and 27,080 estimated observations across the tundra biomes (Fig. 4). There are 27,638 observations from continuous permafrost, 12,905 from discontinuous permafrost, and 8,126 from sporadic permafrost.

- Deleted: to compare
- Deleted: measurements
- Deleted: (CITATION NEEDED)
- Deleted: aggregate to plot level using
- Deleted: submitNm, distur, siteId, plotId, fireYr, and year,
- Deleted: averaged the estimated
- Deleted: , and include the
- Deleted: following variables: submitNm, distur, siteId, plotId, fireYr, year, entryId, lastNm, lat, lon, biome, fireId, paired, gtProde, hitRock, orgDepth, srlH2O, topoPos, slope, vegCvr, estDoy, estDepth, tsf, tsfClass, resBiome, resName, permaExtent, and count
- Deleted: Site c
- Deleted: sites
- Deleted: site
- Deleted: To examine the difference between burned
- Deleted: and unburned sites, measurements were aggregated
- Deleted: ecozone (‘resName’),
- Formatted: Font: 10 pt, Font color: Black
- Deleted: 47,952
- Deleted: 9,432
- Deleted: 794
- Deleted: 19,338
- Deleted: 434
- Deleted: 12,587
- Deleted: 28
- Deleted: 76
- Deleted: 376
- Deleted: 8981
- Deleted: 495
- Deleted: 22,500
- Deleted: 27,257
- Deleted: 27,201
- Deleted: 13,798
- Deleted: 8,758

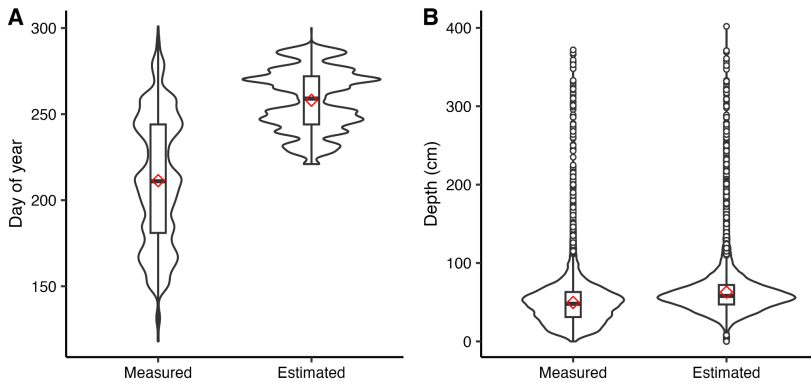


**Figure 5.** The distribution for *in situ* measurements vs. estimated measurements. For day of year (A) and thaw depth (B), we show the distribution for *in situ* measurements vs. estimated measurements using violin plots overlain with boxplots with a red diamond marking the mean. Measured day of year and depths were provided in the raw data contribution. The day of year shows a wide spread of dates, which is caused by the broad geographic extent of the data. Estimated values were calculated to create a dataset that characterises maximum thaw depth (i.e., ALT).

### 3.2 Estimated ALT

The estimated ALT provides a temporally consistent measurement capable of quantifying the effects of wildfire on active layer dynamics temporally and spatially. The data show the shift from measured thaw depth to estimated ALT characterised by a narrower range of dates and depth measurements (Fig. 5A & 5B). The day of year is condensed for the estimated measures (Fig. 5A), which was anticipated since the contributed data were collected throughout the thawing season resulting in a wide spread due to the broad geographic extent of the data whereas the estimated data were truncated to the later part of the thaw season, resulting in a narrow range of days. The uncertainty in the estimated ALT varies with biome and disturbance (Table 5, Fig. 6). Boreal burned values tend to underestimate by about five percent, whereas unburned values tend to overestimate by about 15 percent. For the tundra, burned and unburned values tend to be overestimated by 19.6 and 22.8 percent respectively. The sample size is much smaller for the tundra biome for estimating uncertainty.

**Table 5.** Quantifying uncertainty for estimated ALT. We report the root mean square error (RMSE), percent uncertainty, mean residual error as an indication of bias, and sample size for burned and unburned sites in the validation dataset. Negative values indicate an overestimation and positive values indicate an underestimation.

Biome	Disturbance	RMSE	Percent uncertainty	Mean residual error (bias)	Sample size
Boreal	Burned	22.8	4.6	5.7	413



Boreal	Unburned	20.3	14.5	-8.4	212
Tundra	Burned	29.2	19.6	13.9	20
Tundra	Unburned	5.6	22.8	12.5	6

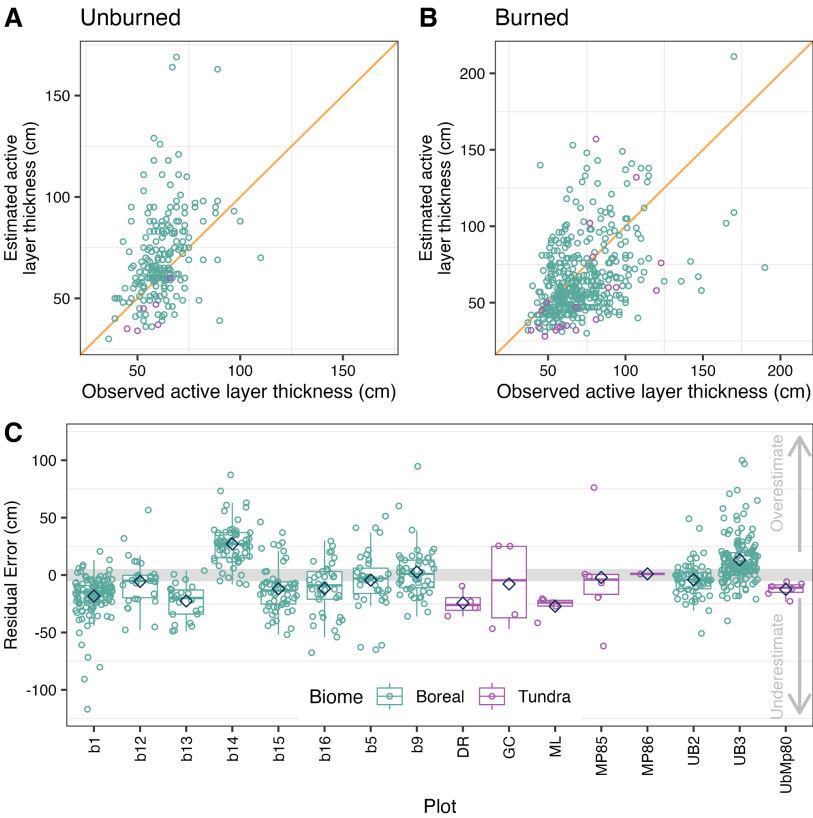


Figure 6. Quantifying uncertainty of ALT estimates. Panel (A) and (B) show observed depths compared to estimated depths split by unburned and burned sites with the orange line showing a slope of one. Panel (C) shows the bias by plot identifier, where zero indicates no difference between the observed and estimated values. Negative values indicate an underestimation and positive values indicate an overestimation with the mean shown by the blue diamond. Burned sites include b1, b12, b13, b14, b15, b16, b5, b9, DR, GC, ML, MP85, and MP86, and unburned sites are ub2, ub3, and UbMp80.

Deleted: U

Deleted: plots

422

423 **3.3 Difference in estimated ALT between burned and unburned sites**

424 By aggregating the burned and unburned pairings, we show the percent difference in estimated ALT between burned and  
425 unburned sites post-fire (Fig. 7, S3, S4). Most sites show a thickening of the active layer post-fire compared to adjacent  
426 unburned sites. Generally, across boreal sites the mean percent difference shows a thickening of the active layer in the two  
427 decades following fire, followed by a recovery in the subsequent decades (e.g., time since fire 21-40 and >40). The magnitude  
428 of difference varies by biome and permafrost extent. In the boreal forest continuous permafrost region, the means follow this  
429 general trend of expansion followed by recovery, however, there is very limited and no data at 4-10 years and >40 years,  
430 respectively. The boreal forest discontinuous permafrost region follows the general trend, whereas the boreal forest sporadic  
431 permafrost region shows a lower percent difference in the two decades following fire where the active layer does expand but  
432 not to the same extent as seen in the continuous or discontinuous permafrost following a varied recovery at 21-40 and >40  
433 years. The tundra biome follows the same general trend that the boreal sites do where mean percent difference shows a  
434 thickening of the active layer in the two decades following fire, followed by a recovery in the subsequent decades (e.g., time  
435 since fire 21-40 and >40). This trend is most distinct for tundra sites with continuous permafrost, whereas sites with  
436 discontinuous permafrost show a bit more variability for 11-20, 21-40, and >40 years. The tundra sites with discontinuous  
437 permafrost have a sample of one for 21-40 and >40 years, which makes it challenging to fully understand the recovery trend.  
438 The trend of post-fire thickening of the active layer followed by recovery illustrates the effect of climate on permafrost  
439 recovery. The variability in the extent of the thickening of the active layer across permafrost zones might provide insight to  
440 potential future patterns. Specifically, the reduced thickening seen in the warmer boreal sporadic region might be a future  
441 pattern that we see extending to the boreal discontinuous zone as the climate continues to warm.

442

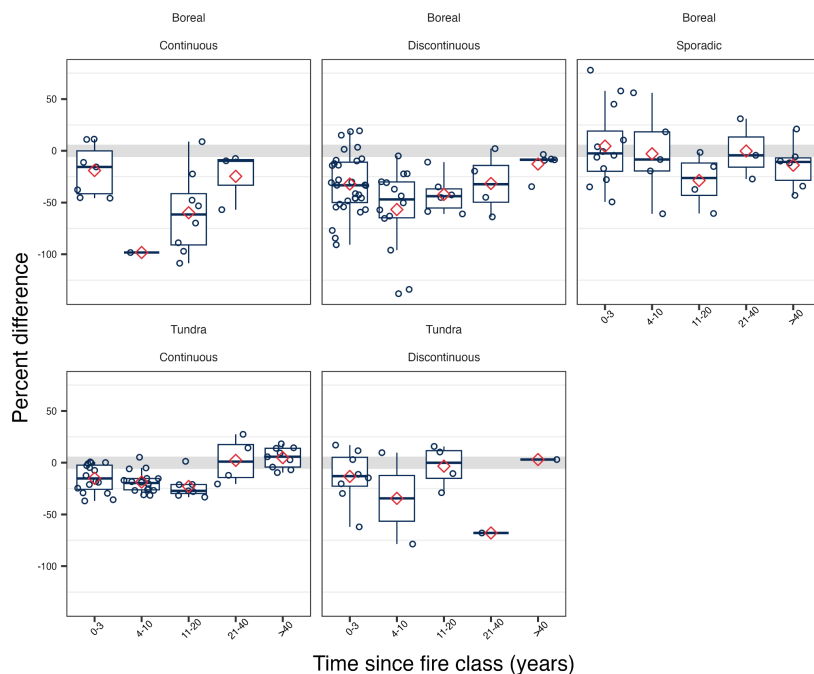


**Figure 7. Percent difference in estimated ALT between burned and unburned paired sites in the years following wildfire. The percent difference is calculated  $(\text{unburned} - \text{burned}) / ((\text{unburned} + \text{burned}) / 2) * 100$ . Negative values indicate that the burned sites have a thicker active layer than the unburned site, while values around zero show little difference in ALT, and positive values indicate that unburned sites have a thicker active layer than the burned ALT. The red diamond indicates the mean based on paired burned-unburned and then aggregated by time since fire class, permafrost extent, and biome. The box and whisker plots show the split in quantiles. See Supplemental Materials to see a similar plot by ecozone (Fig. S3 and S4).**

## 4 Strengths, Limitations, and Opportunities

### 4.1 Strengths

The FireALT dataset (Talucci et al., 2024) offers paired burned and unburned sites that can be aggregated and viewed both spatially and temporally to provide critical insights for understanding wildfire impacts on ALT, a feature commonly used to determine permafrost conditions. Field data collection is often spatially and temporally opportunistic, making comparisons of disparate datasets difficult. For example, several geographically similar sites had depth measurements collected across a wide

range of dates throughout August and September, but these measurements were not necessarily capturing the maximum ALT and therefore not comparable. Further, it is challenging to compare early to end of season thaw depth measurements (Holloway and Lewkowicz 2020). By estimating ALT, the data can be used to extrapolate beyond individual measurements and provide broader understanding of spatial and temporal feedbacks between wildfires, permafrost, and climate. Additionally, data include several environment attributes, e.g., organic layer depth, slope, topographic position, and whether surface water was present. Future analyses could integrate these environmental variables to expound upon the relationship between environmental variables, ALT, and wildfire. Finally, we show a general expansion of the active layer following fire followed by recovery 40 years post-fire but the magnitude of expansion and recovery vary by biome and permafrost zone, pointing to the role of vegetation, permafrost conditions, and climate on active layer dynamics in response to wildfire (Brown et al., 2015). Climate has changed over the time period of the fire events captured within this dataset. Generally, the data indicates that we may expect the active layer to fully recover 40 years post-fire, but that may change for more recent fires. The boreal sporadic zone experiences less expansion of the active layer with a less distinct recovery, which demonstrates how climate influences active layer recovery in warmer regions. This illustrates how climate influences permafrost recovery, and with a warming climate, we may expect to see patterns more like this in boreal discontinuous permafrost zone.

4.2 Limitations, uncertainty, and bias

Estimating ALT is crucial for spatial-temporal evaluations of wildfire-permafrost interactions due to the variability in thaw depth throughout the thaw season. However, uncertainties arise in the estimated ALT from the data we integrate to make those calculations. Air temperature can be a reliable metric for calculating maximum ALT (Osterkamp and Burn 2002, Holloway and Lewkowicz 2020), but the coarse resolution climate data and *in situ* weather station gaps (Clelland et al. 2024), as well as the lack of accounting for disturbance effects on air temperature (Kurylyk and Hayashi, 2016, Muñoz-Sabater et al., 2021, Helbig et al., 2024), all impact the accuracy of the estimated ALT. The Stefan equation assumes negligible soil heat capacity and thus can overestimate thaw depth, and it also does not account for fire altering the surface energy balance (e.g., reducing albedo, loss of canopy and shading) and heat fluxes (e.g., loss of above-ground biomass), all of which increase thaw depths and can contribute to underestimations of ALT (Kurylyk and Hayashi, 2016). Our quantification of uncertainty supports this underestimation bias for burned sites and over estimation for unburned sites in the boreal biome. Further, the lack of inclusion of frozen water content in the Stefan equation may affect early season measurements due to the zero curtain, where the rate of thawing may not scale directly with air temperature (Osterkamp, 1987, Romanovsky and Osterkamp, 2000). These effects likely vary between tundra and boreal sites. These are dynamic systems with multiple feedbacks that influence the freeze-thaw cycle and the timing of maximum thaw depth. Similarly, the time at which permafrost begins to refreeze from the bottom varies with permafrost temperature, soil moisture and thermal properties, and local edaphic hydrological conditions. Consequently, our assumption that ALT occurs 14 days before the date at which air temperature drops below freezing is

Formatted: Normal

another source of uncertainty. Overall, interannual variability in ALT is dependent on complex interactions between air temperature, precipitation, snow dynamics, hydrothermal processes, water energy exchanges, and fluctuations in thaw season length, which are a source of uncertainty in our approach (Shur et al., 2005, Hu et al., 2023, Grünberg et al., 2024). While in warmer boreal sites the 14 day lag may be longer or non-existent depending on the complex interactions of these landscape-level controls. Despite this, estimating ALT allows for insightful comparisons between sites that are not appropriate or meaningful with the raw data.

Deleted: I

Deleted: Although there are uncertainties

Deleted: valuable

Deleted: feasible

Burn severity is a critical component of wildfire that impacts ALT and permafrost stability through combustion of the insulating organic matter, vegetation and post-fire changes in albedo (Rocha and Shaver 2011, Alexander et al., 2018). We do not account for burn severity in the data, which could strongly influence differences we see between burned and unburned ALT. Burn severity could be estimated using the organic depth measurement in the data, but the organic depth will be influenced by time since fire or through the integration of satellite imagery that could be used as a proxy for burn severity. However, vegetation indices that estimate burn severity (e.g., differenced Normalized Burn Ratio [dNBR]) are typically better correlated with aboveground burn severity while less indicative of burn depth (e.g., Delcourt et al., 2021). Recent research which has shown combinations of remote sensing proxies, dNBR, and land surface temperature could be used in conjunction with these field measurements to estimate changes in ALT across fire scars (Diaz et al., 2024). Additionally, the ice content of permafrost may impact the interaction between wildfire and permafrost, with direct effects on ALT particularly where subsidence is involved or where the increase in ALT contributes to the degradation of ice-rich permafrost (e.g., Yedomia) in the short-term (Nelson et al., 2021, Strauss et al., 2021, Jones et al., 2024). Subsidence is not accounted for in the synthesised data. Subsidence can introduce additional bias in the measurement of ALT since thaw depth probing uses the surface as a reference. In areas where subsidence had occurred after fire, our data set will underestimate the magnitude of active layer thickening caused by fire. Bias from subsidence is difficult to estimate because it would be spatially heterogeneous, temporarily nonlinear, and largely dependent on ice content (Shiklomanov et al., 2010, O'Neill et al., 2023, Painter et al., 2023).

Formatted: Font: Not Bold

Formatted: Font: Not Bold

Deleted: would be

Formatted: Font: Not Bold

Formatted: Font: Not Bold

Deleted: (CITATION NEEDED).

Formatted: Font: Not Bold

Formatted: Font: Not Bold

Formatted: Font: Not Bold

Deleted: (CITATION NEEDED)

In addition to these physical controls, there are additional biogeomorphic factors that influence changes in ALT from fire. Landscape scale variation in topography, soil type and moisture, ground ice content, and vegetation cover and regrowth are all sources of uncertainty that cannot be accounted for in our synthesised dataset (Shiklomanov et al., 2010, O'Neill et al., 2023, Painter et al., 2023) accounting for these drivers would require datasets that may or may not be available, and is a separate research effort outside the scope of this paper. We use ecozones to highlight summary statistics of the data set since ecozones are characterised by sharing similar climates, geologic substrates, vegetation, and landforms. The use of ecozones for providing a broad overview of the data, which captures some of the variability in ALT measurements; however, finer-scale landscape features likely still add substantial variation to the estimated ALT and changes from fire. Future work could analyze how microtopographic features that influence local hydrology, burn severity, vegetation structure and function, and ice content impact wildfire-induced changes in ALT. Further, while growing season lengths and thawing degree days have increased over

Deleted: The use of ecozones for providing a broad overview of the data hopefully minimises some of these biases, however, finer scale landscape features likely still contribute to uncertainties in the estimated ALT. Accounting for such microtopographic features that may influence local hydrology, burn severity, vegetation structure and function, and ice content is not feasible.

536 the last century (e.g., Barichivich et al., 2012), the data synthesised here was only measured from 2001 onward despite covering  
537 fire events from 1900-2022. Recent thaw depth measurements from areas that burned more than several decades ago represent  
538 a post-fire evolution of the active layer under climatic conditions that no longer exist. The snapshot of thaw depth related to  
539 wildfire events in space and time provided by this data set may therefore include climatic effects that are hard to disentangle.  
540 Warming trends in the northern high-latitudes have influenced cryoturbation (e.g., Liu et al., 2024), which may bias the  
541 estimated ALT.

542 **4.3 Representativeness of the data**

543 The data included in our dataset are predominantly from North America, and there are large spatial gaps across the northern  
544 high latitude permafrost region (Fig. S5). For example, Russia is underrepresented despite containing 65% of the northern  
545 high-latitude permafrost (Anisimov and Reneva 2006, Streletskiy et al., 2019) and a majority of the burned area within the  
546 northern permafrost region (Loranty et al., 2016). The lack of data for this region is further exacerbated by the Russian invasion  
547 of Ukraine (López-Blanco et al., 2024), which has impacted international collaborations. Additionally, some of the spatial  
548 gaps could be a function of the submission criteria that required a burned/unburned pair. Due to the remoteness of northern  
549 high latitude fires, field campaigns may be constrained spatially and temporally based on accessibility of field sites and timing  
550 of field campaigns. Opportunistic site selection introduces bias into the dataset; however, this is unavoidable for the data  
551 synthesis effort that relies on contributions of existing data.

552 **4.4 Future research opportunities**

553 There is opportunity to expand this dataset to increase the spatio-temporal coverage of the data to better understand impacts  
554 of wildfire on permafrost dynamics. While we touch on how ALT differs across burned and unburned sites across the northern  
555 high latitude permafrost zone, further investigation is warranted on the role of wildfire on permafrost dynamics. We have  
556 identified several understudied research areas that could be augmented with this dataset. First, the dataset could be used to  
557 further investigate the geospatial distribution of permafrost recovery following fire across the northern high latitude permafrost  
558 zone. Second, these data could be used to determine the probability (i.e., likelihood) of permafrost recovery after wildfire as a  
559 function of ecotype or ecoclimatic zone, permafrost classification, fire rotation period, and/or climate. Third, the data could  
560 aid in determining the soil C consequences of temporary or permanent post-fire permafrost degradation. Fourth, investigations  
561 could be structured to identify changes in wildfire activity that affects the likelihood of permafrost recovery/degradation and  
562 associated soil C vulnerability using predictive mapping. Fifth, the data could be used to develop an organic layer deficit value  
563 that would represent the difference between the organic layer thickness in the burn scar with the organic layer thickness in the  
564 unburned control site. Sixth, this dataset could be augmented with quantification of subsidence and the combination of that  
565 with ALT to understand how much new permafrost is exposed to seasonal thaw as a result of fire. Finally, there is the  
566 opportunity for this dataset to be used in algorithm development, calibration, and validation for evolving process-based models  
567 that are trying to capture the impact of fires on permafrost.

Deleted: (

Deleted: CITATION NEEDED)

Formatted: Font: Not Bold

Formatted: Font: Not Bold

Formatted: Font: Not Bold

Commented [2]: Move?

Deleted: (CITATION NEEDED)

Deleted: .

Formatted: Font: Not Bold

Formatted: Font: Not Bold

Deleted: ¶

573 **5 Data use guidelines & availability**

574 The FireALT dataset (Talucci et al., 2024) are publicly available for download through the Arctic Data Center under a Creative  
575 Commons Attribution 4.0 International copyright (CC BY 4.0). Data should be appropriately referenced by citing this paper  
576 and the dataset (see Arctic Data Center). Users of the data are invited to ask questions by contacting the dataset developers.  
577 We recommend that researchers planning to use this data as a core portion of their analysis collaborate with the data developers  
578 and relevant individual site contributors. The data are available for download as a csv file through the Arctic Data Center  
579 (<https://doi.org/10.18739/A2RN3092P>).

Deleted: [10.18739/A2W950Q33](https://doi.org/10.18739/A2W950Q33)

582 **6 Conclusions**

583 The FireALT dataset offers a collection of paired burned and unburned sites with measured thaw depths and estimated ALT.  
584 By estimating ALT, we address a key challenge: the ability to assess impacts of wildfire on ALT when measurements are  
585 taken at various times throughout the thaw season depending on the time of field campaigns (typically June through August).  
586 This dataset can be utilised for future research activities that can expand understanding of the feedbacks between permafrost,  
587 wildfire, and global climate systems. Changes to the active layer serve as an important diagnostic indicator that requires  
588 continuous monitoring under the current dynamic climate conditions to further understand temporary or permanent changes to  
589 permafrost and subsequent losses in carbon storage. These types of data synthesis efforts are crucial for addressing  
590 understudied research areas particularly algorithm development, calibration, and validation for evolving process-based models  
591 as well as extrapolating across space and time, which will elucidate permafrost-wildfire interactions under accelerated warming  
592 across the high northern latitude permafrost zone.

593 **Author contributions**

594 The FireALT dataset was conceptualised during the 2019 Permafrost Carbon Network meeting by ACT, BMR, DO, KLM,  
595 LTB, MAW, MJL, MML with additional input by ACT, AKP, AVR, BMR, JAO, JEH, KLM, LTB, MAW, MJL, MRT, NB,  
596 REH, SMN, SV for the methods. Data curation was carried out by AB, ACT, AKP, AS, AVR, BB, BVG, CJFD, CM, CMD,  
597 DO, GVF, HDA, JAO, JEH, JLB, KLM, LB, LBS, LRD, LTB, MCM, MML, MRT, MTJ, NB, OS, RAL, REH, SMN, SS,  
598 SV, TAD, TAS, TH. Formal analysis was performed by ACT, JEH, MML. ACT and MML provided project management.  
599 BMR, MML provided supervision. Visualisations were created by ACT, JEH, JD. ACT, JEH, MML wrote the original draft.  
600 All authors contributed to the realisation of the permafrost wildfire data and participated in the editing of the manuscript.  
601

603     **Competing Interests**

604     S. Veraverbeke is a member of the editorial board of ESSD. The contact author declares that they and all other co-authors have  
605     no competing interests.  
606

607     **Acknowledgments**

608     A. C. Talucci acknowledges Christina Shintani and Greg Fiske at Woodwell Climate Research Center for their cartographic  
609     feedback and funding support from the NSF Arctic System Science (award no. 2116864). J. E. Holloway acknowledges Antoni  
610     Lewkowicz at the University of Ottawa for the support for field data collections. B.M. Rogers recognizes support from the  
611     Gordon and Betty Moore Foundation (grant no. 8414), NSF Arctic System Science (award no. 2116864), and funding  
612     catalysed by the Audacious Project (Permafrost Pathways). J. O'Donnell acknowledges Jennifer Harden and support from the  
613     U.S. Geological Survey for field data collections. D. Olefeldt acknowledges Carolyn Gibson for her field work contributions  
614     to the contributed data. L. T. Berner was supported by the NASA Arctic Boreal Vulnerability Experiment (80NSSC22K1244  
615     & 80NSSC22K1247). S.M. Natali acknowledges John Wood and the Polaris Project team for field support, and funding from  
616     NSF (1417700, 1915307, 1561437) and NASA (NNX15AT81A). T.A. Douglas acknowledges the U.S. Department of  
617     Defense's Strategic Environmental Research and Development Program (Project RC18- 1170) and Environmental Science  
618     and Technology Certification Program (Project RC22-D3-7408) as well as the U.S. Army Engineer Research and Development  
619     Center Basic Research Portfolio through Program Element PE 0601102A/T14/ST1409. S. Sistla and N. Baillargeon  
620     acknowledge support from NSF 2218742. J.L. Baltzer acknowledges funding through the Government of the Northwest  
621     Territories' Cumulative Impacts Monitoring Program Project 170, Canada First Research Excellence Fund's Global Water  
622     Futures program (project Northern Water Futures), Natural Sciences and Engineering Research Council's Discovery Grant  
623     funding, and the Canada Research Chairs program. Data collection was conducted under Aurora Research Institute's Scientific  
624     Research License numbers 16815, 16755, 16311, 16018, 15879, and 15609. C. J. F. Delcourt acknowledges funding from the  
625     Dutch Research Council (NWO) through a Vidi grant (grant no. 016.Vidi.189.070) and from the European Research Council  
626     (ERC) through a Consolidator grant under the European Union's Horizon 2020 research and innovation program (grant no.  
627     101000987), both awarded to S. Veraverbeke. T. A. Shestakova acknowledges funding from the Beatriu de Pinòs Programme  
628     of the Government of Catalonia (2020 BP 00126). K. Manies acknowledges the support of the U.S. Geological Survey Earth  
629     Surface Dynamics Program. A.K. Paulson and H. D. Alexander acknowledge Seth Robinson, Eric Borth, Sarah Frankenberg,  
630     Aaron Lewis, Brian Izbicki, Clark Thompson, Jill Young, Amanda Ruland, and Elena Forbath for assistance with field work  
631     and Valetin Spektor, Nikita Zimov, Sergei Davydov, and Sergei Zimov for contributing extensive knowledge of the region  
632     and logistics support. We also acknowledge NSF OPP-2100773. G. V. Frost acknowledges funding from the Western Alaska  
633     Landscape Conservation Cooperative (WALCC) award F16AC01215, NASA Arctic Boreal Vulnerability Experiment contract  
634     NNH16CP09C. B.V. Gaglioti acknowledges Park Williams for fieldwork, and NSF Award 2124824 and the Joint Fire Science



635 Program Project 20-2-01-13 for funding. Thanks to Benjamin Maglio and Dana Brown for their assistance in reviewing this  
636 manuscript. Thanks to the Arctic Data Center team for their assistance with archiving the dataset. Any use of trade, firm, or  
637 product names is for descriptive purposes only and does not imply endorsement by the U.S. Government.  
638

## 639 References

- 640 Alexander, H. D., Natali, S. M., Loranty, M. M., Ludwig, S. M., Spektor, V. V., Davydov, S., Zimov, N., Trujillo, I., and  
641 Mack, M. C.: Impacts of increased soil burn severity on larch forest regeneration on permafrost soils of far northeastern Siberia,  
642 *Forest Ecology and Management*, 417, 144–153, <https://doi.org/10.1016/j.foreco.2018.03.008>, 2018.  
643
- 644 Alexander, H. D., Paulson, A. K., DeMarco, J., Hewitt, R., Lichstein, J., Loranty, M. M., Mack, M. C., McEwan, R.,  
645 Frankenberg, S., and Robinson, S.: Fire influences on forest recovery and associated climate feedbacks in Siberian Larch  
646 Forests, Russia, 2018–2019, <https://doi.org/10.18739/A2XG9FB90>, 2020.  
647
- 648 Amiro, B. D.: Paired-tower measurements of carbon and energy fluxes following disturbance in the boreal forest, *Global*  
649 *Change Biology*, 7, 253–268, <https://doi.org/10.1046/j.1365-2486.2001.00398.x>, 2001.  
650
- 651 Amiro, B. D., Orchansky, A. L., Barr, A. G., Black, T. A., Chambers, S. D., Chapin Iii, F. S., Goulden, M. L., Litvak, M., Liu,  
652 H. P., McCaughey, J. H., McMillan, A., and Randerson, J. T.: The effect of post-fire stand age on the boreal forest energy  
653 balance, *Agricultural and Forest Meteorology*, 140, 41–50, <https://doi.org/10.1016/j.agrformet.2006.02.014>, 2006.  
654
- 655 Anisimov, O. and Reneva, S.: Permafrost and Changing Climate: The Russian Perspective, *AMBIO: A Journal of the Human*  
656 *Environment*, 35, 169–175, [https://doi.org/10.1579/0044-7447\(2006\)35\[169:PACCTR\]2.0.CO;2](https://doi.org/10.1579/0044-7447(2006)35[169:PACCTR]2.0.CO;2), 2006.  
657
- 658 Baillargeon, N., Pold, G., Natali, S. M., and Sistla, S. A.: Lowland tundra plant stoichiometry is somewhat resilient decades  
659 following fire despite substantial and sustained shifts in community structure, *Arctic, Antarctic, and Alpine Research*, 54, 525–  
660 536, <https://doi.org/10.1080/15230430.2022.2121246>, 2022.  
661
- 662 Baltzer, J. L., Veness, T., Chasmer, L. E., Sniderhan, A. E., and Quinton, W. L.: Forests on thawing permafrost: fragmentation,  
663 edge effects, and net forest loss, *Global Change Biology*, 20, 824–834, <https://doi.org/10.1111/gcb.12349>, 2014.  
664

665 [Barichivich, J., Briffa, K. R., Osborn, T. J., Melvin, T. M., and Caesar, J.: Thermal growing season and timing of biospheric](#)  
666 [carbon uptake across the Northern Hemisphere, \*Global Biogeochemical Cycles\*, 26, 2012GB004312,](#)  
667 <https://doi.org/10.1029/2012GB004312>, 2012.

668

669 Bonnaventure, P. P. and Lamoureux, S. F.: The active layer: A conceptual review of monitoring, modeling techniques and  
670 changes in a warming climate, *Progress in Physical Geography: Earth and Environment*, 37, 352–376,  
671 <https://doi.org/10.1177/0309133313478314>, 2013.

672

673 Bret-Harte, M. S., Mack, M. C., Shaver, G. R., Huebner, D. C., Johnston, M., Mojica, C. A., Pizano, C., and Reiskind, J. A.:  
674 The response of Arctic vegetation and soils following an unusually severe tundra fire, *Phil. Trans. R. Soc. B*, 368, 20120490,  
675 <https://doi.org/10.1098/rstb.2012.0490>, 2013.

676

677 Brown, D. R. N., Jorgenson, M. T., Douglas, T. A., Romanovsky, V. E., Kielland, K., Hiemstra, C., Euskirchen, E. S., and  
678 Ruess, R. W.: Interactive effects of wildfire and climate on permafrost degradation in Alaskan lowland forests, *JGR*  
679 *Biogeosciences*, 120, 1619–1637, <https://doi.org/10.1002/2015JG003033>, 2015.

680

681 Brown, J., Ferrians, O., Heginbottom, J. A., and Melnikov, E.: Circum-Arctic Map of Permafrost and Ground-Ice Conditions,  
682 Version 2 [Data Set], <https://doi.org/10.7265/skbg-kf16>, 1998.

683

684 Brown, J., Hinkel, K. M., and Nelson, F. E.: The circumpolar active layer monitoring (calm) program: Research designs and  
685 initial results, *Polar Geography*, 24, 166–258, <https://doi.org/10.1080/10889370009377698>, 2000.

686

687 Byrne, B., Liu, J., Bowman, K. W., Pascolini-Campbell, M., Chatterjee, A., Pandey, S., Miyazaki, K., Van Der Werf, G. R.,  
688 Wunch, D., Wennberg, P. O., Roehl, C. M., and Sinha, S.: Carbon emissions from the 2023 Canadian wildfires, *Nature*, 633,  
689 835–839, <https://doi.org/10.1038/s41586-024-07878-z>, 2024.

690

691 Burn, C. R. and Lewkowicz, A. G.: Canadian Landform Examples - 17: Retrogressive thaw slumps, *Canadian Geographies /*  
692 *Géographies canadiennes*, 34, 273–276, <https://doi.org/10.1111/j.1541-0064.1990.tb01092.x>, 1990.

693

694 Calvin, K., Dasgupta, D., Krinner, G., Mukherji, A., Thorne, P. W., Trisos, C., Romero, J., Aldunce, P., Barrett, K., Blanco,  
695 G., Cheung, W. W. L., Connors, S., Denton, F., Diongue-Niang, A., Dodman, D., Garschagen, M., Geden, O., Hayward, B.,  
696 Jones, C., Jotzo, F., Lasco, R., Lee, Y.-Y., Masson-Delmotte, V., Meinshausen, M., Mintenbeck, K., Mokssit, A.,  
697 Otto, F. E. L., Pathak, M., Pirani, A., Poloczanska, E., Pörtner, H.-O., Revi, A., Roberts, D. C., Roy, J., Ruane, A. C., Skea, J.,  
698 Shukla, P. R., Slade, R., Slangen, A., Sokona, Y., Sörensson, A. A., Tignor, M., Van Vuuren, D., Wei, Y.-M., Winkler, H.,

699 Zhai, P., Zommers, Z., Hourcade, J.-C., Johnson, F. X., Pachauri, S., Simpson, N. P., Singh, C., Thomas, A., Totin, E., Arias,  
700 P., Bustamante, M., Elgizouli, I., Flato, G., Howden, M., Méndez-Vallejo, C., Pereira, J. J., Pichs-Madruga, R., Rose, S. K.,  
701 Saheb, Y., Sánchez Rodríguez, R., Ürge-Vorsatz, D., Xiao, C., Yassaa, N., Alegría, A., Armour, K., Bednar-Friedl, B., Blok,  
702 K., Cissé, G., Dentener, F., Eriksen, S., Fischer, E., Garner, G., Guivarch, C., Haasnoot, M., Hansen, G., Hauser, M., Hawkins,  
703 E., Hermans, T., Kopp, R., Leprince-Ringuet, N., Lewis, J., Ley, D., Ludden, C., Niamir, L., Nicholls, Z., Some, S., Szopa, S.,  
704 Trewin, B., Van Der Wijst, K.-I., Winter, G., Witting, M., Birt, A., Ha, M., et al.: IPCC, 2023: Climate Change 2023: Synthesis  
705 Report. Contribution of Working Groups I, II and III to the Sixth Assessment Report of the Intergovernmental Panel on Climate  
706 Change [Core Writing Team, H. Lee and J. Romero (eds.)]. IPCC, Geneva, Switzerland., Intergovernmental Panel on Climate  
707 Change (IPCC), <https://doi.org/10.59327/IPCC/AR6-9789291691647>, 2023.

708

709 Chambers, S. D., Beringer, J., Randerson, J. T., and Chapin, F. S.: Fire effects on net radiation and energy partitioning:  
710 Contrasting responses of tundra and boreal forest ecosystems, *J. Geophys. Res.*, 110, 2004JD005299,  
711 <https://doi.org/10.1029/2004JD005299>, 2005.

712

713 Chambers, S. D. and Chapin, F. S.: Fire effects on surface-atmosphere energy exchange in Alaskan black spruce ecosystems:  
714 Implications for feedbacks to regional climate, *J. Geophys. Res.*, 107, <https://doi.org/10.1029/2001JD000530>, 2002.

715

716 [Chebykina, E., Polyakov, V., Abakumov, E., and Petrov, A.: Wildfire Effects on Cryosols in Central Yakutia Region, Russia,](#)  
717 [Atmosphere, 13, 1889, https://doi.org/10.3390/atmos13111889, 2022.](#)

718

719 Clelland, A. A., Marshall, G. J., and Baxter, R.: Evaluating the performance of key ERA-INTERIM , ERA5 and ERA5-LAND  
720 climate variables across Siberia, *Intl Journal of Climatology*, 44, 2318–2342, <https://doi.org/10.1002/joc.8456>, 2024.

721

722 Dearborn, K. D., Wallace, C. A., Patankar, R., and Baltzer, J. L.: Permafrost thaw in boreal peatlands is rapidly altering forest  
723 community composition, *Journal of Ecology*, 109, 1452–1467, <https://doi.org/10.1111/1365-2745.13569>, 2021.

724

725 de Groot, W. J., Flannigan, M. D., and Cantin, A. S.: Climate change impacts on future boreal fire regimes, *Forest Ecology*  
726 *and Management*, 294, 35–44, <https://doi.org/10.1016/j.foreco.2012.09.027>, 2013.

727

728 Delcourt, C. J. F., Combee, A., Izbicki, B., Mack, M. C., Maximov, T., Petrov, R., Rogers, B. M., Scholten, R. C., Shestakova,  
729 T. A., Van Wees, D., and Veraverbeke, S.: Evaluating the Differenced Normalized Burn Ratio for Assessing Fire Severity  
730 Using Sentinel-2 Imagery in Northeast Siberian Larch Forests, *Remote Sensing*, 13, 2311, <https://doi.org/10.3390/rs13122311>,  
731 2021.

732

733 Delcourt, C. J. F., Rogers, B. M., Akhmetzyanov, L., Izbicki, B., Scholten, R. C., Shestakova, T., van Wees, D., Mack, M. C.,  
734 Sass-Klaassen, U., and Veraverbeke, S.: Burned and Unburned Boreal Larch Forest Site Data, Northeast Siberia,  
735 <https://doi.org/10.5281/zenodo.10840088>, 2024.

736

737 Derksen, C., Burgess, D., Duguay, C., Howell, S., Mudryk, L., Smith, S., Thackeray, C., and Kirchmeier-Young, M.: Changes  
738 in snow, ice, and permafrost across Canada, in: Canada's Changing Climate Report, Government of Canada, Ottawa, Ontario,  
739 194–260, 2019.

740

741 Descals, A., Gaveau, D. L. A., Verger, A., Sheil, D., Naito, D., and Peñuelas, J.: Unprecedented fire activity above the Arctic  
742 Circle linked to rising temperatures, *Science*, 378, 532–537, <https://doi.org/10.1126/science.abn9768>, 2022.

743

744 Diaz, L. R., Delcourt, C. J. F., Langer, M., Loranty, M. M., Rogers, B. M., Scholten, R. C., Shestakova, T. A., Talucci, A. C.,  
745 Vonk, J. E., Wangchuk, S., and Veraverbeke, S.: Environmental drivers and remote sensing proxies of post-fire thaw depth in  
746 Eastern Siberian larch forests, <https://doi.org/10.5194/egusphere-2024-469>, 21 March 2024.

747

748 Dieleman, C.M., Day, N.J., Holloway, J.E., Baltzer, J., Douglas, T.A., Turetsky, M.R.. Carbon and nitrogen cycling dynamics  
749 following permafrost thaw in the Northwest Territories, 845, 157288, <https://doi-org/10.1016/j.scitotenv.2022.157288>, 2022

750 ▼

751 Dinerstein, E., Olson, D., Joshi, A., Vynne, C., Burgess, N. D., Wikramanayake, E., Hahn, N., Palminteri, S., Hedao, P., Noss,  
752 R., Hansen, M., Locke, H., Ellis, E. C., Jones, B., Barber, C. V., Hayes, R., Kormos, C., Martin, V., Crist, E., Sechrest, W.,  
753 Price, L., Baillie, J. E. M., Weeden, D., Suckling, K., Davis, C., Sizer, N., Moore, R., Thau, D., Birch, T., Potapov, P.,  
754 Turubanova, S., Tyukavina, A., De Souza, N., Pintea, L., Brito, J. C., Llewellyn, O. A., Miller, A. G., Patzelt, A., Ghazanfar,  
755 S. A., Timberlake, J., Klöser, H., Shennan-Farpon, Y., Kindt, R., Lillesø, J.-P. B., Van Breugel, P., Gaudal, L., Voge, M., Al-  
756 Shammari, K. F., and Saleem, M.: An Ecoregion-Based Approach to Protecting Half the Terrestrial Realm, *BioScience*, 67,  
757 534–545, <https://doi.org/10.1093/biosci/bix014>, 2017.

758

759 Douglas, T. A., Jorgenson, M. T., Brown, D. R. N., Campbell, S. W., Hiemstra, C. A., Saari, S. P., Bjella, K., and Liljedahl,  
760 A. K.: Degrading permafrost mapped with electrical resistivity tomography, airborne imagery and LiDAR, and seasonal thaw  
761 measurements, *GEOPHYSICS*, 81, WA71–WA85, <https://doi.org/10.1190/geo2015-0149.1>, 2016.

762

763 Douglas, T. A., Turetsky, M. R., and Koven, C. D.: Increased rainfall stimulates permafrost thaw across a variety of Interior  
764 Alaskan boreal ecosystems, *npj Clim Atmos Sci*, 3, 28, <https://doi.org/10.1038/s41612-020-0130-4>, 2020.

765

766 [Fedorov, A. N.: Permafrost Landscape Research in the Northeast of Eurasia, \*Earth\*, 3, 460–478,  
767 <https://doi.org/10.3390/earth3010028>, 2022.](https://doi.org/10.3390/earth3010028)

Deleted: ¶

769

770 Fisher, J. P., Estop-Aragónés, C., Thierry, A., Charman, D. J., Wolfe, S. A., Hartley, I. P., Murton, J. B., Williams, M., and  
771 Phoenix, G. K.: The influence of vegetation and soil characteristics on active-layer thickness of permafrost soils in boreal  
772 forest, *Glob Change Biol*, 22, 3127–3140, <https://doi.org/10.1111/gcb.13248>, 2016.

773

774 Fraser, R., Kokelj, S., Lantz, T., McFarlane-Winchester, M., Olthof, I., and Lacelle, D.: Climate Sensitivity of High Arctic  
775 Permafrost Terrain Demonstrated by Widespread Ice-Wedge Thermokarst on Banks Island, *Remote Sensing*, 10, 954,  
776 <https://doi.org/10.3390/rs10060954>, 2018.

777

778 Freitag, D. and McFadden, T.: *Introduction to Cold Regions Engineering*, 166–169, 1997.

779

780 Frost, G. V., Loehman, R. A., Nelson, P. R., and Paradis, D. P.: ABoVE: Vegetation Composition across Fire History Gradients  
781 on the Y-K Delta, Alaska, <https://doi.org/10.3334/ORNLDAAC/1772>, 2020.

782

783 Gaglioti, B. V., Berner, L. T., Jones, B. M., Orndahl, K. M., Williams, A. P., Andreu-Hayles, L., D’Arrigo, R. D., Goetz, S.  
784 J., and Mann, D. H.: Tussocks Enduring or Shrubs Greening: Alternate Responses to Changing Fire Regimes in the Noatak  
785 River Valley, Alaska, *J Geophys Res Biogeosci*, 126, <https://doi.org/10.1029/2020JG006009>, 2021.

786

787 Gasser, T., Kechiar, M., Ciaia, P., Burke, E. J., Kleinen, T., Zhu, D., Huang, Y., Ekici, A., and Obersteiner, M.: Path-dependent  
788 reductions in CO<sub>2</sub> emission budgets caused by permafrost carbon release, *Nature Geosci*, 11, 830–835,  
789 <https://doi.org/10.1038/s41561-018-0227-0>, 2018.

790

791 Gibson, C. M., Brinkman, T., Cold, H., Brown, D., and Turetsky, M.: Identifying increasing risks of hazards for northern land-  
792 users caused by permafrost thaw: integrating scientific and community-based research approaches, *Environ. Res. Lett.*, 16,  
793 064047, <https://doi.org/10.1088/1748-9326/abfc79>, 2021.

794

795 Gibson, C. M., Chasmer, L. E., Thompson, D. K., Quinton, W. L., Flannigan, M. D., and Olefeldt, D.: Wildfire as a major  
796 driver of recent permafrost thaw in boreal peatlands, *Nat Commun*, 9, 3041, <https://doi.org/10.1038/s41467-018-05457-1>,  
797 2018.

798

799 Gorelick, N., Hancher, M., Dixon, M., Ilyushchenko, S., Thau, D., and Moore, R.: Google Earth Engine: Planetary-scale  
800 geospatial analysis for everyone, *Remote Sensing of Environment*, 202, 18–27, <https://doi.org/10.1016/j.rse.2017.06.031>,  
801 2017.

802

803 [Grünberg, L., Groenke, B., Westermann, S., and Boike, J.: Permafrost and Active Layer Temperature and Freeze/Thaw Timing](#)  
804 [Reflect Climatic Trends at Bayelva, Svalbard, JGR Earth Surface, 129, e2024JF007648,](#)  
805 <https://doi.org/10.1029/2024JF007648>, 2024.

806

807 Hanes, C. C., Wang, X., Jain, P., Parisien, M.-A., Little, J. M., and Flannigan, M. D.: Fire-regime changes in Canada over the  
808 last half century, *Can. J. For. Res.*, 49, 256–269, <https://doi.org/10.1139/cjfr-2018-0293>, 2019.

809

810 Harden, J. W., Manies, K. L., Turetsky, M. R., and Neff, J. C.: Effects of wildfire and permafrost on soil organic matter and  
811 soil climate in interior Alaska: EFFECTS OF WILDFIRE AND PERMAFROST ON SOIL, *Global Change Biology*, 12, 2391–  
812 2403, <https://doi.org/10.1111/j.1365-2486.2006.01255.x>, 2006.

813

814 Harris, S. A. and Permafrost Subcommittee, Associate Committee on Geotechnical Research, National Research Council of  
815 Canada (Eds.): *Glossary of permafrost and related ground-ice terms*, Ottawa, Ontario, Canada, 156 pp., 1988.

816

817 Hayes, K. and Buma, B.: Effects of short-interval disturbances continue to accumulate, overwhelming variability in local  
818 resilience, *Ecosphere*, 12, e03379, <https://doi.org/10.1002/ecs2.3379>, 2021.

819

820 [Heim, R. J., Bucharova, A., Brodt, L., Kamp, J., Rieker, D., Soromotin, A. V., Yurtaev, A., and Hölzel, N.: Post-fire vegetation](#)  
821 [succession in the Siberian subarctic tundra over 45 years, Science of The Total Environment, 760, 143425,](#)  
822 <https://doi.org/10.1016/j.scitotenv.2020.143425>, 2021.

823

824 Helbig, M., Daw, L., Iwata, H., Rudaitis, L., Ueyama, M., and Živković, T.: Boreal Forest Fire Causes Daytime Surface  
825 Warming During Summer to Exceed Surface Cooling During Winter in North America, *AGU Advances*, 5, e2024AV001327,  
826 <https://doi.org/10.1029/2024AV001327>, 2024.

827

828 Hollingsworth, T. N., Breen, A. L., Hewitt, R. E., and Mack, M. C.: Does fire always accelerate shrub expansion in Arctic  
829 tundra? Examining a novel grass-dominated successional trajectory on the Seward Peninsula, Arctic, Antarctic, and Alpine  
830 Research, 53, 93–109, <https://doi.org/10.1080/15230430.2021.1899562>, 2021.

831

832 Hollingsworth, T. N., Breen, A., Mack, M. C., and Hewitt, R. E.: Seward Peninsula post-fire vegetation and soil data from  
833 multiple burns occurring from 1971 to 2012: “SPANFire” Study Sites, 2020.

834

835 Holloway, J.: Impacts of forest fire on permafrost in the discontinuous zones of northwestern Canada, University of Ottawa,  
836 Ottawa, Ontario, 2020.

837

Holloway, J. E. and Lewkowicz, A. G.: Half a century of discontinuous permafrost persistence and degradation in western Canada, *Permafrost and Periglac Process*, 31, 85–96, <https://doi.org/10.1002/ppp.2017>, 2020.

Holloway, J. E., Lewkowicz, A. G., Douglas, T. A., Li, X., Turetsky, M. R., Baltzer, J. L., and Jin, H.: Impact of wildfire on permafrost landscapes: A review of recent advances and future prospects, *Permafrost and Periglac Process*, 31, 371–382, <https://doi.org/10.1002/ppp.2048>, 2020.

Hu, G., Zhao, L., Li, R., Wu, X., Wu, T., Zou, D., Zhu, X., Jie, C., Su, Y., Hao, J., and Li, W.: Dynamics of the freeze–thaw front of active layer on the Qinghai-Tibet Plateau, *Geoderma*, 430, 116353, <https://doi.org/10.1016/j.geoderma.2023.116353>, 2023.

Huang, B., Lu, F., Wang, X., Zheng, H., Wu, X., Zhang, L., Yuan, Y., and Ouyang, Z.: Ecological restoration is crucial in mitigating carbon loss caused by permafrost thawing on the Qinghai-Tibet Plateau, *Commun Earth Environ*, 5, 341, <https://doi.org/10.1038/s43247-024-01511-7>, 2024.

Hugelius, G., Strauss, J., Zubrzycki, S., Harden, J. W., Schuur, E. A. G., Ping, C.-L., Schirmer, L., Grosse, G., Michaelson, G. J., Koven, C. D., O'Donnell, J. A., Elberling, B., Mishra, U., Camill, P., Yu, Z., Palmtag, J., and Kuhry, P.: Estimated stocks of circumpolar permafrost carbon with quantified uncertainty ranges and identified data gaps, *Biogeosciences*, 11, 6573–6593, <https://doi.org/10.5194/bg-11-6573-2014>, 2014.

Jafarov, E. E., Romanovsky, V. E., Genet, H., McGuire, A. D., and Marchenko, S. S.: The effects of fire on the thermal stability of permafrost in lowland and upland black spruce forests of interior Alaska in a changing climate, *Environ. Res. Lett.*, 8, 035030, <https://doi.org/10.1088/1748-9326/8/3/035030>, 2013.

Jiang, Y., Rocha, A. V., O'Donnell, J. A., Drysdale, J. A., Rastetter, E. B., Shaver, G. R., and Zhuang, Q.: Contrasting soil thermal responses to fire in Alaskan tundra and boreal forest: Contrasting soil thermal responses, *J. Geophys. Res. Earth Surf.*, 120, 363–378, <https://doi.org/10.1002/2014JF003180>, 2015.

Jones, B. M., Grosse, G., Arp, C. D., Miller, E., Liu, L., Hayes, D. J., and Larsen, C. F.: Recent Arctic tundra fire initiates widespread thermokarst development, *Sci Rep*, 5, 15865, <https://doi.org/10.1038/srep15865>, 2015.

Jones, B. M., Kanevskiy, M. Z., Shur, Y., Gaglioti, B. V., Jorgenson, M. T., Ward Jones, M. K., Veremeeva, A., Miller, E. A., and Jandt, R.: Post-fire stabilization of thaw-affected permafrost terrain in northern Alaska, *Sci Rep*, 14, 8499, <https://doi.org/10.1038/s41598-024-58998-5>, 2024.

873 Kasischke, E. S., Verbyla, D. L., Rupp, T. S., McGuire, A. D., Murphy, K. A., Jandt, R., Barnes, J. L., Hoy, E. E., Duffy, P.  
874 A., Calef, M., and Turetsky, M. R.: Alaska's changing fire regime — implications for the vulnerability of its boreal forests.  
875 *Can. J. For. Res.*, 40, 1313–1324, <https://doi.org/10.1139/X10-098>, 2010.

876

877 Kirdyanov, A. V., Saurer, M., Siegwolf, R., Knorre, A. A., Prokushkin, A. S., Churakova (Sidorova), O. V., Fonti, M. V., and  
878 Büntgen, U.: Long-term ecological consequences of forest fires in the continuous permafrost zone of Siberia, *Environ. Res.  
879 Lett.*, 15, 034061, <https://doi.org/10.1088/1748-9326/ab7469>, 2020.

880

881 Knoblauch, C., Beer, C., Liebner, S., Grigoriev, M. N., and Pfeiffer, E.-M.: Methane production as key to the greenhouse gas  
882 budget of thawing permafrost, *Nature Clim Change*, 8, 309–312, <https://doi.org/10.1038/s41558-018-0095-z>, 2018.

883

884 Kurylyk, B. L. and Hayashi, M.: Improved Stefan Equation Correction Factors to Accommodate Sensible Heat Storage during  
885 Soil Freezing or Thawing, *Permafrost & Periglacial*, 27, 189–203, <https://doi.org/10.1002/ppp.1865>, 2016.

886

887 Lewkowicz, A. G.: Dynamics of active-layer detachment failures, Fosheim Peninsula, Ellesmere Island, Nunavut, Canada,  
888 *Permafrost & Periglacial*, 18, 89–103, <https://doi.org/10.1002/ppp.578>, 2007.

889

890 Li, X., Jin, H., He, R., Huang, Y., Wang, H., Luo, D., Jin, X., Lü, L., Wang, L., Li, W., Wei, C., Chang, X., Yang, S., and Yu,  
891 S.: Effects of forest fires on the permafrost environment in the northern Da Xing'anling (Hinggan) mountains, Northeast China,  
892 *Permafrost & Periglacial*, 30, 163–177, <https://doi.org/10.1002/ppp.2001>, 2019.

893

894 Liljedahl, A. K., Boike, J., Daanen, R. P., Fedorov, A. N., Frost, G. V., Grosse, G., Hinzman, L. D., Iijma, Y., Jorgenson, J.  
895 C., Matveyeva, N., Necsoiu, M., Reynolds, M. K., Romanovsky, V. E., Schulla, J., Tape, K. D., Walker, D. A., Wilson, C. J.,  
896 Yabuki, H., and Zona, D.: Pan-Arctic ice-wedge degradation in warming permafrost and its influence on tundra hydrology,  
897 *Nature Geosci*, 9, 312–318, <https://doi.org/10.1038/ngeo2674>, 2016.

898

899 Liu, H., Randerson, J. T., Lindfors, J., and Chapin, F. S.: Changes in the surface energy budget after fire in boreal ecosystems  
900 of interior Alaska: An annual perspective, *J. Geophys. Res.*, 110, 2004JD005158, <https://doi.org/10.1029/2004JD005158>,  
901 2005.

902

903 [Liu, L., Zhuang, Q., Zhao, D., Wei, J., and Zheng, D.: The Fate of Deep Permafrost Carbon in Northern High Latitudes in the](#)  
904 [21st Century: A Process-Based Modeling Analysis, \*Earth's Future\*, 12, e2024EF004996,](#)  
905 <https://doi.org/10.1029/2024EF004996>, 2024.

906

**Deleted:** This article is one of a selection of papers from The Dynamics of Change in Alaska's Boreal Forests: Resilience and Vulnerability in Response to Climate Warming.,



910 López-Blanco, E., Topp-Jørgensen, E., Christensen, T. R., Rasch, M., Skov, H., Arndal, M. F., Bret-Harte, M. S., Callaghan,  
 911 T. V., and Schmidt, N. M.: Towards an increasingly biased view on Arctic change, *Nat. Clim. Chang.*, 14, 152–155,  
 912 <https://doi.org/10.1038/s41558-023-01903-1>, 2024.  
 913  
 914 Loranty, M. M., Lieberman-Cribbin, W., Berner, L. T., Natali, S. M., Goetz, S. J., Alexander, H. D., and Kholodov, A. L.:  
 915 Spatial variation in vegetation productivity trends, fire disturbance, and soil carbon across arctic-boreal permafrost ecosystems,  
 916 *Environ. Res. Lett.*, 11, 095008, <https://doi.org/10.1088/1748-9326/11/9/095008>, 2016.  
 917  
 918 [Lytkina, L.: Post-fire dynamics of forest growth conditions in larch forests of Central Yakutia. \*Geogr. Nat. Resour.\*, 2, 181–](#)  
 919 [185, 2008.](#)  
 920  
 921 Mamet, S. D., Chun, K. P., Kershaw, G. G. L., Loranty, M. M., and Peter Kershaw, G.: Recent Increases in Permafrost Thaw  
 922 Rates and Areal Loss of Palsas in the Western Northwest Territories, Canada, *Permafrost & Periglacial*, 28, 619–633,  
 923 <https://doi.org/10.1002/ppp.1951>, 2017.  
 924  
 925 McCarty, J. L., Aalto, J., Paunu, V.-V., Arnold, S. R., Eckhardt, S., Klimont, Z., Fain, J. J., Evangeliou, N., Venäläinen, A.,  
 926 Tchepakova, N. M., Parfenova, E. I., Kupiainen, K., Soja, A. J., Huang, L., and Wilson, S.: Reviews and syntheses: Arctic fire  
 927 regimes and emissions in the 21st century, *Biogeosciences*, 18, 5053–5083, <https://doi.org/10.5194/bg-18-5053-2021>, 2021.  
 928  
 929 [Moskalenko, N.G. Anthropogenic Dynamics of Vegetation in the Plains of the Russian Permafrost; Nauka: Novosibirsk,](#)  
 930 [Russia, 1999; p. 280. \(In Russian\)](#)  
 931  
 932 Muñoz Sabater, J.: ERA5-Land Daily Aggregated- ECMWF Climate Reanalysis, <https://doi.org/10.24381/cds.68d2bb30>,  
 933 2019.  
 934  
 935 Muñoz-Sabater, J., Dutra, E., Agustí-Panareda, A., Albergel, C., Arduini, G., Balsamo, G., Boussetta, S., Choulga, M.,  
 936 Harrigan, S., Hersbach, H., Martens, B., Miralles, D. G., Piles, M., Rodríguez-Fernández, N. J., Zsoter, E., Buontempo, C.,  
 937 and Thépaut, J.-N.: ERA5-Land: a state-of-the-art global reanalysis dataset for land applications, *Earth Syst. Sci. Data*, 13,  
 938 4349–4383, <https://doi.org/10.5194/essd-13-4349-2021>, 2021.  
 939  
 940 Natali, S.: Yukon-Kuskokwim Delta fire: thaw depth, soil temperature, and point-intercept vegetation, Yukon-Kuskokwim  
 941 Delta Alaska, 2015-2019., <https://doi.org/10.18739/A2707WP16>, 2018.  
 942  
 943 Natali, S., Kholodov, A. L., and Loranty, M. M.: Thaw depth and organic layer depth from Alaska borehole sites, 2015, 2017,  
 944 2018 (ViPER Project), <https://doi.org/10.18739/A22J6848J>, 2016.

945  
 946 Natali, S., Ludwig, S., Minions, C., and Watts, J. D.: ABoVE: Thaw Depth at Selected Unburned and Burned Sites Across  
 947 Alaska, 2016-2017., <https://doi.org/0.3334/ORNLDAAAC/1579..> 2018, 2018.  
 948  
 949 Natali, S. M., Holdren, J. P., Rogers, B. M., Treharne, R., Duffy, P. B., Pomerance, R., and MacDonald, E.: Permafrost carbon  
 950 feedbacks threaten global climate goals, *Proc. Natl. Acad. Sci. U.S.A.*, 118, e2100163118,  
 951 <https://doi.org/10.1073/pnas.2100163118>, 2021.  
 952  
 953 Nelson, F. E., Shiklomanov, N. I., and Nyland, K. E.: Cool, CALM, collected: the Circumpolar Active Layer Monitoring  
 954 program and network, *Polar Geography*, 44, 155–166, <https://doi.org/10.1080/1088937X.2021.1988001>, 2021.  
 955  
 956 Nossov, D. R., Torre Jorgenson, M., Kielland, K., and Kanevskiy, M. Z.: Edaphic and microclimatic controls over permafrost  
 957 response to fire in interior Alaska, *Environ. Res. Lett.*, 8, 035013, <https://doi.org/10.1088/1748-9326/8/3/035013>, 2013.  
 958  
 959 O'Donnell, J. A., Harden, J. W., and Manies, K. L.: Soil physical, chemical, and gas flux characterization from *Picea mariana*  
 960 stands near Erickson Creek, Alaska., U.S. Geological Survey, 2011a.  
 961  
 962 O'Donnell, J. A., Harden, J. W., Manies, K. L., Jorgenson, M. T., and Kanevskiy, M. Z.: Soil data from fire and permafrost-  
 963 thaw chronosequences in upland *Picea mariana* stands near Hess Creek and Tok, Alaska., US Geological Survey, 2013.  
 964  
 965 O'Donnell, J. A., Harden, J. W., McGUIRE, A. D., Kanevskiy, M. Z., Jorgenson, M. T., and Xu, X.: The effect of fire and  
 966 permafrost interactions on soil carbon accumulation in an upland black spruce ecosystem of interior Alaska, *Global Change*  
 967 *Biology*, 17, 1461–1474, <https://doi.org/10.1111/j.1365-2486.2010.02358.x>, 2011b.  
 968  
 969 O'Donnell, J. A., Harden, J. W., McGuire, A. D., and Romanovsky, V. E.: Exploring the sensitivity of soil carbon dynamics  
 970 to climate change, fire disturbance and permafrost thaw in a black spruce ecosystem, *Biogeosciences*, 8, 1367–1382,  
 971 <https://doi.org/10.5194/bg-8-1367-2011>, 2011c.  
 972  
 973 O'Neill, H. B., Smith, S. L., Burn, C. R., Duchesne, C., and Zhang, Y.: Widespread Permafrost Degradation and Thaw  
 974 Subsidence in Northwest Canada, *JGR Earth Surface*, 128, e2023JF007262, <https://doi.org/10.1029/2023JF007262>, 2023.  
 975  
 976 Osterkamp, T. E.: Freezing and thawing of soils and permafrost containing unfrozen water or brine, *Water Resources Research*,  
 977 23, 2279–2285, <https://doi.org/10.1029/WR023i012p02279>, 1987.  
 978

979 Osterkamp, T. E. and Burn, C. R.: Permafrost, in: Encyclopedia of Atmospheric Sciences, Academic Press, 2002.

980

981 [Painter, S. L., Coon, E. T., Khattak, A. J., and Jastrow, J. D.: Drying of tundra landscapes will limit subsidence-induced](#)

982 [acceleration of permafrost thaw, Proc. Natl. Acad. Sci. U.S.A., 120, e2212171120, <https://doi.org/10.1073/pnas.2212171120>,](#)

983 [2023.](#)

984

985

986 Peng, X., Zhang, T., Frauenfeld, O. W., Mu, C., Wang, K., Wu, X., Guo, D., Luo, J., Hjort, J., Aalto, J., Karjalainen, O., and

987 Luoto, M.: Active Layer Thickness and Permafrost Area Projections for the 21st Century, Earth's Future, 11, e2023EF003573,

988 <https://doi.org/10.1029/2023EF003573>, 2023.

989

990 [Petrov, M. I., Fedorov, A. N., Konstantinov, P. Y., and Argunov, R. N.: Variability of Permafrost and Landscape Conditions](#)

991 [Following Forest Fires in the Central Yakutian Taiga Zone, Land, 11, 496, <https://doi.org/10.3390/land11040496>, 2022.](#)

992

993 Phillips, C. A., Rogers, B. M., Elder, M., Cooperdock, S., Moubarak, M., Randerson, J. T., and Frumhoff, P. C.: Escalating

994 carbon emissions from North American boreal forest wildfires and the climate mitigation potential of fire management, Sci.

995 Adv., 8, eabl7161, <https://doi.org/10.1126/sciadv.abl7161>, 2022.

996

997 Rantanen, M., Kämäräinen, M., Niittynen, P., Phoenix, G. K., Lenoir, J., Maclean, I., Luoto, M., and Aalto, J.: Bioclimatic

998 atlas of the terrestrial Arctic, Sci Data, 10, 40, <https://doi.org/10.1038/s41597-023-01959-w>, 2023.

999

1000 Rocha, A. V., Lorant, M. M., Higuera, P. E., Mack, M. C., Hu, F. S., Jones, B. M., Breen, A. L., Rastetter, E. B., Goetz, S.

1001 J., and Shaver, G. R.: The footprint of Alaskan tundra fires during the past half-century: implications for surface properties

1002 and radiative forcing, Environ. Res. Lett., 7, 044039, <https://doi.org/10.1088/1748-9326/7/4/044039>, 2012.

1003

1004 Rocha, A. V. and Shaver, G. R.: Postfire energy exchange in arctic tundra: the importance and climatic implications of burn

1005 severity, Global Change Biology, 17, 2831–2841, <https://doi.org/10.1111/j.1365-2486.2011.02441.x>, 2011.

1006

1007 Romanovsky, V. E. and Osterkamp, T. E.: Effects of unfrozen water on heat and mass transport processes in the active layer

1008 and permafrost, Permafrost Periglac. Process., 11, 219–239, [https://doi.org/10.1002/1099-1530\(200007/09\)11:3<219::AID-](https://doi.org/10.1002/1099-1530(200007/09)11:3<219::AID-PPP352>3.0.CO;2-7)

1009 [PPP352>3.0.CO;2-7](#), 2000.

1010

1011

1012 Romanovsky, V. E., Smith, S. L., and Christiansen, H. H.: Permafrost thermal state in the polar Northern Hemisphere during  
 1013 the international polar year 2007–2009: a synthesis, *Permafrost & Periglacial*, 21, 106–116, <https://doi.org/10.1002/ppp.689>,  
 1014 2010.  
 1015  
 1016 Rouse, W. R.: Microclimatic Changes Accompanying Burning in Subarctic Lichen Woodland, *Arctic and Alpine Research*, 8,  
 1017 357, <https://doi.org/10.2307/1550439>, 1976.  
 1018  
 1019 Rudy, A. C. A., Lamoureux, S. F., Treitz, P., Ewijk, K. V., Bonnaventure, P. P., and Budkewitsch, P.: Terrain Controls and  
 1020 Landscape-Scale Susceptibility Modelling of Active-Layer Detachments, Sabine Peninsula, Melville Island, Nunavut:  
 1021 Landscape-Scale Modelling of Active-Layer Detachment Susceptibility, *Permafrost and Periglac. Process.*, 28, 79–91,  
 1022 <https://doi.org/10.1002/ppp.1900>, 2017.  
 1023  
 1024 Sannel, A. B. K. and Kuhry, P.: Warming-induced destabilization of peat plateau/thermokarst lake complexes, *J. Geophys.*  
 1025 *Res.*, 116, G03035, <https://doi.org/10.1029/2010JG001635>, 2011.  
 1026  
 1027 Schädel, C., Rogers, B. M., Lawrence, D. M., Koven, C. D., Brovkin, V., Burke, E. J., Genet, H., Huntzinger, D. N., Jafarov,  
 1028 E., McGuire, A. D., Riley, W. J., and Natali, S. M.: Earth system models must include permafrost carbon processes, *Nat. Clim.*  
 1029 *Chang.*, <https://doi.org/10.1038/s41558-023-01909-9>, 2024.  
 1030  
 1031 Schaefer, K., Lantuit, H., Romanovsky, V. E., Schuur, E. A. G., and Witt, R.: The impact of the permafrost carbon feedback  
 1032 on global climate, *Environ. Res. Lett.*, 9, 085003, <https://doi.org/10.1088/1748-9326/9/8/085003>, 2014.  
 1033  
 1034 [Scheer, J., Caduff, R., How, P., Marcer, M., Strozzi, T., Bartsch, A., and Ingeman-Nielsen, T.: Thaw-Season InSAR Surface](#)  
 1035 [Displacements and Frost Susceptibility Mapping to Support Community-Scale Planning in Ilulissat, West Greenland, Remote](#)  
 1036 [Sensing](#), 15, 3310, <https://doi.org/10.3390/rs15133310>, 2023.  
 1037  
 1038 Scholten, R. C., Coumou, D., Luo, F., and Veraverbeke, S.: Early snowmelt and polar jet dynamics co-influence recent extreme  
 1039 Siberian fire seasons, *Science*, 378, 1005–1009, <https://doi.org/10.1126/science.abn4419>, 2022.  
 1040  
 1041 Schuur, E. A. G., McGuire, A. D., Schädel, C., Grosse, G., Harden, J. W., Hayes, D. J., Hugelius, G., Koven, C. D., Kuhry,  
 1042 P., Lawrence, D. M., Natali, S. M., Olefeldt, D., Romanovsky, V. E., Schaefer, K., Turetsky, M. R., Treat, C. C., and Vonk, J.  
 1043 E.: Climate change and the permafrost carbon feedback, *Nature*, 520, 171–179, <https://doi.org/10.1038/nature14338>, 2015.  
 1044  
 1045 Schuur, E. A. G., Abbott, B. W., Commane, R., Ernakovich, J., Euskirchen, E., Hugelius, G., Grosse, G., Jones, M., Koven,  
 1046 C., Leshyk, V., Lawrence, D., Lorant, M. M., Mauritz, M., Olefeldt, D., Natali, S., Rodenhizer, H., Salmon, V., Schädel, C.,

1047 Strauss, J., Treat, C., and Turetsky, M.: Permafrost and Climate Change: Carbon Cycle Feedbacks From the Warming Arctic,  
1048 Annu. Rev. Environ. Resour., 47, 343–371, <https://doi.org/10.1146/annurev-environ-012220-011847>, 2022.

1049

1050 See, C. R., Virkkala, A.-M., Natali, S. M., Rogers, B. M., Mauritz, M., Biasi, C., Bokhorst, S., Boike, J., Bret-Harte, M. S.,  
1051 Celis, G., Chae, N., Christensen, T. R., Murner, S. J., Dengel, S., Dolman, H., Edgar, C. W., Elberling, B., Emmerton, C. A.,  
1052 Euskirchen, E. S., Göckede, M., Grelle, A., Heffernan, L., Helbig, M., Holl, D., Humphreys, E., Iwata, H., Järveoja, J.,  
1053 Kobayashi, H., Kochendorfer, J., Kolari, P., Kotani, A., Kutzbach, L., Kwon, M. J., Lathrop, E. R., López-Blanco, E.,  
1054 Mammarella, I., Marushchak, M. E., Mastepanov, M., Matsuura, Y., Merbold, L., Meyer, G., Minions, C., Nilsson, M. B.,  
1055 Nojeim, J., Oberbauer, S. F., Olefeldt, D., Park, S.-J., Parmentier, F.-J. W., Peichl, M., Peter, D., Petrov, R., Poyatos, R.,  
1056 Prokushkin, A. S., Quinton, W., Rodenhizer, H., Sachs, T., Savage, K., Schulze, C., Sjögersten, S., Sonnentag, O., St. Louis,  
1057 V. L., Torn, M. S., Tuittila, E.-S., Ueyama, M., Varlagin, A., Voigt, C., Watts, J. D., Zona, D., Zyryanov, V. I., and Schuur,  
1058 E. A. G.: Decadal increases in carbon uptake offset by respiratory losses across northern permafrost ecosystems, Nat. Clim.  
1059 Chang., 14, 853–862, <https://doi.org/10.1038/s41558-024-02057-4>, 2024.

1060

1061 Shiklomanov, N. I., Streletskiy, D. A., Nelson, F. E., Hollister, R. D., Romanovsky, V. E., Tweedie, C. E., Bockheim, J. G.,  
1062 and Brown, J.: Decadal variations of active-layer thickness in moisture-controlled landscapes, Barrow, Alaska, J. Geophys.  
1063 Res., 115, G00I04, <https://doi.org/10.1029/2009JG001248>, 2010.

1064

1065 Shur, Y., Hinkel, K. M., and Nelson, F. E.: The transient layer: implications for geocryology and climate-change science,  
1066 Permafrost & Periglacial, 16, 5–17, <https://doi.org/10.1002/ppp.518>, 2005.

1067

1068 Sizov, O., Soromotin, A., and Brodt, L.: Temperature of the active layer in the forest-tundra zone in the north of Western  
1069 Siberia (Pangody) forest-tundra zone in the north of Western Siberia, <https://doi.org/10.5281/zenodo.4285650>, 2020.

1070

1071 Smith, S. L. and Burgess, M.: Sensitivity of permafrost to climate warming in Canada, Natural Resources Canada, 2004.

1072

1073 Smith, S. L., Romanovsky, V. E., Lewkowicz, A. G., Burn, C. R., Allard, M., Clow, G. D., Yoshikawa, K., and Throop, J.:  
1074 Thermal state of permafrost in North America: a contribution to the international polar year, Permafrost & Periglacial, 21,  
1075 117–135, <https://doi.org/10.1002/ppp.690>, 2010.

1076

1077 Smith, S. L., Riseborough, D. W., and Bonnaventure, P. P.: Eighteen Year Record of Forest Fire Effects on Ground Thermal  
1078 Regimes and Permafrost in the Central Mackenzie Valley, NWT, Canada, Permafrost & Periglacial, 26, 289–303,  
1079 <https://doi.org/10.1002/ppp.1849>, 2015.

1081 [Strand, S. M., Christiansen, H. H., Johansson, M., Åkerman, J., and Humlum, O.: Active layer thickening and controls on](#)  
1082 [interannual variability in the Nordic Arctic compared to the circum-Arctic, \*Permafrost & Periglacial\*, 32, 47–58,](#)  
1083 <https://doi.org/10.1002/ppp.2088>, 2021.  
1084

1085 Strauss, J., Laboor, S., Schirrmeister, L., Fedorov, A. N., Fortier, D., Froese, D., Fuchs, M., Günther, F., Grigoriev, M., Harden,  
1086 J., Hugelius, G., Jongejans, L. L., Kanevskiy, M., Kholodov, A., Kunitsky, V., Kraev, G., Lozhkin, A., Rivkina, E., Shur, Y.,  
1087 Siegert, C., Spektor, V., Streletskaia, I., Ulrich, M., Vartanyan, S., Veremeeva, A., Anthony, K. W., Wetterich, S., Zimov, N.,  
1088 and Grosse, G.: Circum-Arctic Map of the Yedoma Permafrost Domain, *Front. Earth Sci.*, 9, 758360,  
1089 <https://doi.org/10.3389/feart.2021.758360>, 2021.  
1090

1091 Streletskiy, D. A., Suter, L. J., Shiklomanov, N. I., Porfiriev, B. N., and Eliseev, D. O.: Assessment of climate change impacts  
1092 on buildings, structures and infrastructure in the Russian regions on permafrost, *Environ. Res. Lett.*, 14, 025003,  
1093 <https://doi.org/10.1088/1748-9326/aaf5e6>, 2019.  
1094

1095 Talucci, A., Loranty, M., Holloway, J., Rogers, B., Alexander, H., Baillargeon, N., Baltzer, J., Berner, L., Breen, A., Brodt,  
1096 L., Buma, B., Delcourt, C., Diaz, L., Dieleman, C., Douglas, T., Frost, G., Gaglioti, B., Hewitt, R., Hollingsworth, T.,  
1097 Jorgenson, M. T., Lara, M., Loehman, R., Mack, M., Manies, K., Minions, C., Natali, S., O'Donnell, J., Olefeldt, D., Paulson,  
1098 A., Rocha, A., Saperstein, L., Shestakova, T., Sistla, S., Oleg, S., Soromotin, A., Turetsky, M., Veraverbeke, S., and Walvoord,  
1099 M.: FireALT dataset: estimated active layer thickness for paired burned unburned sites measured from 2001-2023,  
1100 <https://doi.org/10.18739/A2RN3092P>, 2024.  
1101

1102 [Toevs, G. R., Karl, J. W., Taylor, J. J., Spurrier, C. S., Karl, M. “Sherm,” Bobo, M. R., and Herrick, J. E.: Consistent Indicators](#)  
1103 [and Methods and a Scalable Sample Design to Meet Assessment, Inventory, and Monitoring Information Needs Across Scales,](#)  
1104 [Rangelands](#), 33, 14–20, <https://doi.org/10.2111/1551-501X-33.4.14>, 2011.  
1105

1106 Treharne, R., Rogers, B. M., Gasser, T., MacDonald, E., and Natali, S.: Identifying Barriers to Estimating Carbon Release  
1107 From Interacting Feedbacks in a Warming Arctic, *Front. Clim.*, 3, 716464, <https://doi.org/10.3389/fclim.2021.716464>, 2022.  
1108

1109 Turetsky, M. R., Abbott, B. W., Jones, M. C., Anthony, K. W., Olefeldt, D., Schuur, E. A. G., Grosse, G., Kuhry, P., Hugelius,  
1110 G., Koven, C., Lawrence, D. M., Gibson, C., Sannel, A. B. K., and McGuire, A. D.: Carbon release through abrupt permafrost  
1111 thaw, *Nat. Geosci.*, 13, 138–143, <https://doi.org/10.1038/s41561-019-0526-0>, 2020.  
1112

1113 Wang, Z., Schaaf, C. B., Chopping, M. J., Strahler, A. H., Wang, J., Román, M. O., Rocha, A. V., Woodcock, C. E., and Shuai,  
1114 Y.: Evaluation of Moderate-resolution Imaging Spectroradiometer (MODIS) snow albedo product (MCD43A) over tundra,  
1115 *Remote Sensing of Environment*, 117, 264–280, <https://doi.org/10.1016/j.rse.2011.10.002>, 2012.

Deleted: 10.18739/A2W950Q33

1117  
1118 [Wickham, H., Averick, M., Bryan, J., Chang, W., McGowan, L., François, R., Golemund, G., Hayes, A., Henry, L., Hester,](#)  
1119 [J., Kuhn, M., Pedersen, T., Miller, E., Bache, S., Müller, K., Ooms, J., Robinson, D., Seidel, D., Spinu, V., Takahashi, K.,](#)  
1120 [Vaughan, D., Wilke, C., Woo, K., and Yutani, H.: Welcome to the Tidyverse, JOSS, 4, 1686,](#)  
1121 <https://doi.org/10.21105/joss.01686>, 2019.

1122

1123 Wotton, B. M., Flannigan, M. D., and Marshall, G. A.: Potential climate change impacts on fire intensity and key wildfire  
1124 suppression thresholds in Canada, Environ. Res. Lett., 12, 095003, <https://doi.org/10.1088/1748-9326/aa7e6e>, 2017.

1125

1126 Yokohata, T., Saito, K., Ito, A., Ohno, H., Tanaka, K., Hajima, T., and Iwahana, G.: Future projection of greenhouse gas  
1127 emissions due to permafrost degradation using a simple numerical scheme with a global land surface model, Prog Earth Planet  
1128 Sci, 7, 56, <https://doi.org/10.1186/s40645-020-00366-8>, 2020.

1129

1130 York, A., Bhatt, U. S., Gargulinski, E., Grabinski, Z., Jain, P., Soja, A., Thoman, R. L., Ziel, R., Alaska Center for Climate  
1131 Assessment and Policy (U.S.), International Arctic Research Center, United States. National Oceanic and Atmospheric  
1132 Administration. Office of Oceanic and Atmospheric Research, and Cooperative Institute for Research in the Atmosphere (Fort  
1133 Collins, Colo.): Arctic Report Card 2020: Wildland Fire in High Northern Latitudes, <https://doi.org/10.25923/2GEF-3964>,  
1134 2020.

1135

1136 Zhang, Y., Chen, W., and Riseborough, D. W.: Transient projections of permafrost distribution in Canada during the 21st  
1137 century under scenarios of climate change, Global and Planetary Change, 60, 443–456,  
1138 <https://doi.org/10.1016/j.gloplacha.2007.05.003>, 2008.

1139

1140 Zhang, Y., Wolfe, S. A., Morse, P. D., Olthof, I., and Fraser, R. H.: Spatiotemporal impacts of wildfire and climate warming  
1141 on permafrost across a subarctic region, Canada, JGR Earth Surface, 120, 2338–2356, <https://doi.org/10.1002/2015JF003679>,  
1142 2015.

1143

1144 Zheng, B., Ciais, P., Chevallier, F., Yang, H., Canadell, J. G., Chen, Y., Van Der Velde, I. R., Aben, I., Chuvieco, E., Davis,  
1145 S. J., Deeter, M., Hong, C., Kong, Y., Li, H., Li, H., Lin, X., He, K., and Zhang, Q.: Record-high CO<sub>2</sub> emissions from boreal  
1146 fires in 2021, Science, 379, 912–917, <https://doi.org/10.1126/science.ade0805>, 2023.

1147